Atmospheric Research 154 (2015) 39–59

Contents lists available at ScienceDirect

Atmospheric Research

journal homepage: www.elsevier.com/locate/atmos

How well can we estimate error variance of satellite precipitation data around the world?

Abebe S. Gebregiorgis *, Faisal Hossain

Department of Civil and Environmental Engineering, University of Washington, Seattle, WA 98195, United States

ARTICLE INFO

Article history:
Received 25 June 2014
Received in revised form 24 October 2014
Accepted 5 November 2014
Available online 12 November 2014

Keywords:
Satellite precipitation error variance
Topography
Climate
Season
Precipitation rate
Ungauged regions

ABSTRACT

Providing error information associated with existing satellite precipitation estimates is crucial to advancing applications in hydrologic modeling. In this study, we present a method of estimating the square difference prediction of satellite precipitation (hereafter used synonymously with "error variance") using regression model for three satellite precipitation products (3B42RT, CMORPH, and PERSIANN-CCS) using easily available geophysical features and satellite precipitation rate. Building on a suite of recent studies that have developed the error variance models, the goal of this work is to explore how well the method works around the world in diverse geophysical settings. Topography, climate, and seasons are considered as the governing factors to segregate the satellite precipitation uncertainty and fit a nonlinear regression equation as a function of satellite precipitation rate. The error variance models were tested on USA, Asia, Middle East, and Mediterranean region. Rain-gauge based precipitation product was used to validate the error variance of satellite precipitation products. The regression approach yielded good performance skill with high correlation between simulated and observed error variances. The correlation ranged from 0.46 to 0.98 during the independent validation period. In most cases (~85% of the scenarios), the correlation was higher than 0.72. The error variance models also captured the spatial distribution of observed error variance adequately for all study regions while producing unbiased residual error. The approach is promising for regions where missed precipitation is not a common occurrence in satellite precipitation estimation. Our study attests that transferability of model estimators (which help to estimate the error variance) from one region to another is practically possible by leveraging the similarity in geophysical features. Therefore, the quantitative picture of satellite precipitation error over ungauged regions can be discerned even in the absence of ground truth data.

© 2014 Elsevier B.V. All rights reserved.

1. Introduction

Over the past two and half decades, remote sensing based precipitation estimates have experienced tremendous progress in providing the world a cost-effective and reliable ways of measuring precipitation from space (Adler et al., 2003; Huffman et al., 2001; Joyce et al., 2004; Kuligowski, 2002; Kidd et al., 2003; Miller et al., 2001; Sorooshian et al., 2000; Xie et al., 2007). As compared to ground observation system, satellite precipitation measurement technique, by far, is more effective to address the spatial and temporal variability of precipitation over the vast ungauged regions of the earth surface. It avoids the hurdle of geo-political boundaries issues; it covers both the terrestrial and water bodies of the earth; it provides a continuous (uninterrupted) observation irrespective of time (day/night), terrain and weather condition on the ground; it evades high operational cost of in-situ networks; and it delivers information on a near real-time basis.

Despite the obvious, the presence of non-negligible error (hereafter used synonymously with 'uncertainty') in satellite precipitation estimation presents a hurdle to fully implement

* Corresponding author.
E-mail address: abesine2002@gmail.com (A.S. Gebregiorgis).

http://dx.doi.org/10.1016/j.atmosres.2014.11.005
0169-8095/© 2014 Elsevier B.V. All rights reserved.

the product for wide ranges of hydrologic applications (Pan et al., 2010). Since it is an essential prerequisite for hydrologic applications, assessing the uncertainty of satellite precipitation estimate has become important over the last few years. It is important to understand the nature and quantify the magnitude of this uncertainty in order for users to apply the a priori knowledge to scientific research and practical applications. There are many publicly available high resolution satellite precipitation products (Huffman et al., 2007; Joyce et al., 2004; Sorooshian et al., 2000) available at a global scale which are potentially helpful for many scientific investigations and applications (Wu et al., 2012; Su et al., 2011; Pan et al., 2010; Shrestha et al., 2008; Su et al., 2008; Artan et al., 2007; Hong et al., 2006; among others). However, the question that remains is: '*to what level do the end users have the knowledge about the error information associated to these satellite precipitation products?*'

The advantage of knowing error information can be valuable from two perspectives: 1) from data producers or algorithm developers to improve data quality; and 2) from data users to improve data application. Investigating the components of error and enumerating each error individually can help algorithm developers (data producers) comprehend the strengths and weaknesses of their algorithms in a variety of settings, understand the aspects that are in greatest need of improvement, evaluate and monitor the performance of existing algorithms, and finally, assist with evaluating algorithm upgrades. On the other hand, data (end) users need to verify the accuracy of satellite precipitation products before using them for a particular application. A thorough verification of satellite-based precipitation products can provide users with information on the expected errors in a wide range of hydrologic application, so that they can quantify the expected accuracy in the prediction. With the existence of various satellite precipitation products, the users need to know the level of uncertainty in each product and its implication for a given surface hydrologic prediction. Therefore, data producers and end users can work together and allow information to flow both ways for communal advantage.

The source of satellite-derived precipitation uncertainty could arise from retrieval errors such as instrument, measurement and algorithmic biases, and sampling error (Nijssen and Lettenmaier, 2004; Huffman, 1997). It is a very challenging task to quantify the uncertainty of satellite precipitation estimate for many reasons. First, precipitation by itself exhibits random variation to represent the uncertainty with simple mathematical formulations (Wilks, 2011; North et al., 1993). Second, in case of high spatial and temporal resolution, there is a problem of assigning the rain field precisely for true location on the ground (Bellerby and Sun, 2005). Third, due to the nature of indirect measurement of precipitation processes such as by observing cloud-top properties in case of infrared (IR) sensor, and from thermal emission and backscatter signals in case of microwave (MW) sensor (Huffman, et al., 2010). In general, the accuracy of satellite based precipitation estimates depends on several factors: method of retrieval (type of algorithm), the nature of sensor used, the surface condition (ocean or land), and precipitation type and so on. The collected effect of all these factors makes the satellite precipitation estimates inescapably uncertain.

Moreover, to validate satellite precipitation estimates, ground truth data from rain gauge and/or radar observations are indispensable. The main problem, however, is that most parts of the globe are ungauged or has limited in-situ precipitation observation network. On the other hand, the existing observation networks continue to decline worldwide (Stokstad, 1999; Shiklomanov et al., 2002). The absence of in-situ measurement in most parts of the world represents a 'paradoxical' situation for evaluating satellite precipitation estimation uncertainty. Under such a circumstance, conventional validation of satellite precipitation products over these regions is quite impracticable and unrealistic. There is now a need for us to think outside the box for global applications. Therefore, a question we ask in our previous studies (Gebregiorgis and Hossain, 2013a, 2013b; Gebregiorgis et al., 2012) is, '*how can the uncertainties of satellite precipitation be estimated without having ground reference data?*' In fact, this question needs a novel approach to predict satellite precipitation uncertainty around the world.

The aforementioned challenges have already prompted the scientific community to design research strategies and recommendations for future investigations. For example, in a recent workshop conducted from 15 to 17 March 2010 at University of California, Irvine on Advanced Concepts on Remote Sensing of Precipitation at Multiple Scales (http://chrs.web.uci.edu/events/Workshop_Report.pdf), various research priorities and recommendations have recently emerged. Quantification of satellite precipitation uncertainty for different climate regions, storm regimes, surface conditions, seasons, and elevations was one of the major recommendations made by the community for advancing satellite remote sensing of precipitation (Sorooshian et al., 2011).

In line with these strategies, Gebregiorgis and Hossain (2013a) have demonstrated a method of estimating satellite precipitation error variance using readily available geophysical features and satellite precipitation rate for 3B42RT, CMOPRH, and PERSIANN-CCS products over Mississippi and Northwest basins. First, the basins were grouped into different regions based on topography and Köppen climate. Then, the nonlinear regression models were fitted for each region by taking into consideration the season type as shown in Eq. (1).

$$Ev_{i,j,t} = \alpha_{i,j,k}\left(RR_{i,j,t}\right)^{\beta_{i,j,k}} \tag{1}$$

where, i represents the topographic region, j the climate type, t the time at daily scale, and k the season type; Ev denotes pixel's error variance of the same spatial and temporal resolutions with satellite precipitation product; RR means the satellite precipitation estimates; α symbolizes the scaling factor for each topographic, climate region and season; β the same as α, except that it designates the power or exponent estimator of the regression model. In general, the model estimators α and β control the behaviour, shape and growth or decay of the fitted curve of the regression function. In this study, error variance refers to the square of the difference between the estimated and true value (square error).

The study of Gebregiorgis and Hossain (2013a) showed that the total error variance is directly proportional to the satellite precipitation rate, i.e. the value of β is always positive but has a different rate of growth for various topographic and climate regimes. Fundamentally, the seasonal precipitation variability and its type are strongly dictated by topographic and climate. It is, therefore, safe to claim that the use of geophysical features

such as topography, climate, and season is an appropriate strategy for estimation of error variance that builds the platform for more improved techniques in the future.

Furthermore, several other studies addressed the issue of satellite precipitation uncertainty (Yan and Gebremichael, 2009; Gebremichael et al., 2011; Maggioni et al., 2014). Yan and Gebremichael (2009) developed a non-parametric conditional density function that can be applied to generate actual rainfall data from a given satellite rainfall estimates. Even though, the model was developed for coarser temporal and spatial resolutions, the conditional distribution of the generated rainfall data is well represented by the semi-parametric conditional distribution model. In another study, Gebremichael et al. (2011) developed non-parametric error model at fine spatial and temporal scales (0.25°, 3 hourly) that generates the distribution of actual rainfall given satellite rainfall estimates. The model was tested for one year CMOPRH data and it predicted the actual rainfall reasonably well for the southern United States with relative large variation at low and high rainfall rates. However, the applicability of the model at global scale over long period of various satellite datasets needs to be further explored. On a similar concept, Maggioni et al. (2014) proposed an error model framework that computes the probability distribution of reference precipitation from a given high resolution satellite precipitation estimates which eventually helps to calculate the error as difference or ratio between the satellite product and the estimated reference. The PDF was modeled for TMPA-V7 product over Oklahoma region by decomposing the satellite rainfall error into hit, missed, false, and no-error conditions. Similarly, this study is also limited to specific region in which its applicability for global scale needs further investigation.

Building on our recent works, the key issue now is if the regression models can work around the world in a robust manner. The more specific question is, "*To what level can the regression model developed for calibration regions perform in other parts of the globe (validation regions)?*" This study investigates and addresses this important scientific question in order to advance the knowledge of satellite precipitation uncertainty and promote the use of our pragmatic error variance estimation scheme across the globe.

The remaining part of this paper is organized into the following parts. (1) Study regions, data, and methodology of the study; (2) detailed discussion of the results and findings of the study; and (3) summary of the findings and limitation of the study are presented in the next subsequent sections.

2. Study regions, data, and methodology

2.1. Study regions and period

Four different study regions around the world have been selected: The contiguous United States, Monsoon Asia, Middle East, and Mediterranean regions (Fig. 1). The selection of the study regions was driven by the availability of good quality validation data (in-situ precipitation observation data) at a resolution comparable to the satellite precipitation products. Detailed description of the validation/reference data is provided in Table 1.

The contiguous United States (48 adjoining U.S. states, called CONUS) comprises a total area of 3,119,885 mile^2 (8,080,464 km^2), which is 1.58% of the total surface area of the Earth. This region comprises a diverse topography that ranges from 0 to 4500 m above sea level (a.s.l.). The highest elevation is the Rocky Mountains which are located in the west central part of CONUS. The major climates are arid (highland of west-central), temperate (south, east and west coast), and cold (northern part of the CONUS). Tropical and polar climates are not common in the US due to the positioning of the states in terms of latitude (see Fig. 2 for detailed topography and climate features of the regions).

The Monsoon Asia is the largest and most populous region which is located in the eastern and northern hemisphere. This region encompasses the most diverse region both in topography and climate type. All the topography and climate classes (presented in Table 2) are found in this region. The world's highest mountain range (collectively called Himalayas) is located in this region, including the Everest Mountain which is about 8500 m tall above sea level. All six major climate types are also found in the region: tropical, arid, temperate, cold, and polar climate (Fig. 2 and Table 2).

The Mediterranean region encompasses the lands around the Mediterranean Sea (Fig. 1). The topography of the region ranges from the lowest elevation region on land (The Dead Sea) −420 to 2600 m a.s.l. It includes arid, temperate, and cold types of climate. This region is mainly dominated by convective system during warm periods of the year (Lazri et al., 2014). The Middle East is a region that roughly covers Western Asia region. The topography varies from −300 to 2700 m a.s.l and is dominantly characterized by arid climate type.

To embrace the combination of all types of topographic and climate features, USA and part of Asia regions were selected to calibrate the error variance regression model; whereas, the remaining part of Asia, Mediterranean and Middle East regions were chosen to validate the performance of the model on independent area. Due to absence of adequate rain-gauge stations in some parts of Asia and Middle East, four distinct regions were selected for model validation. These regions comprise east of Tibet and Southern part of Himalayas (from Asia) and Southern part of Iran, Jordan and Israel (from Middle East) (Fig. 1, lower panel). Generally, the study period comprised seven years (2003–2007) in which, 2003–2005 was used for calibration and the period from 2006 to 2007 was for validation of the error variance model. Even though the entire USA has been used for model calibration, it has also been considered as an independent validation region due to the independent validation period.

2.2. Data

In this study, the error variance of three satellite precipitation products was estimated: 3B42RT, CMORPH, and PERSIANN-CCS products. 3B42RT, which is one of the NASA's Tropical Precipitation Measurement Mission (TRMM; Huffman et al., 2007) Multi-satellite Precipitation Analysis (TMPA) precipitation products, is produced by merging high quality Passive Microwave (PMW, 3B40) and PMW calibrated IR estimate (3B41). The product is available at 0.25° spatial resolution and 3 hourly temporal resolutions. It has global coverage between 50° N and 50° S latitude.

CMORPH precipitation product is generated mostly from low orbiting satellites producing high quality PMW estimates.

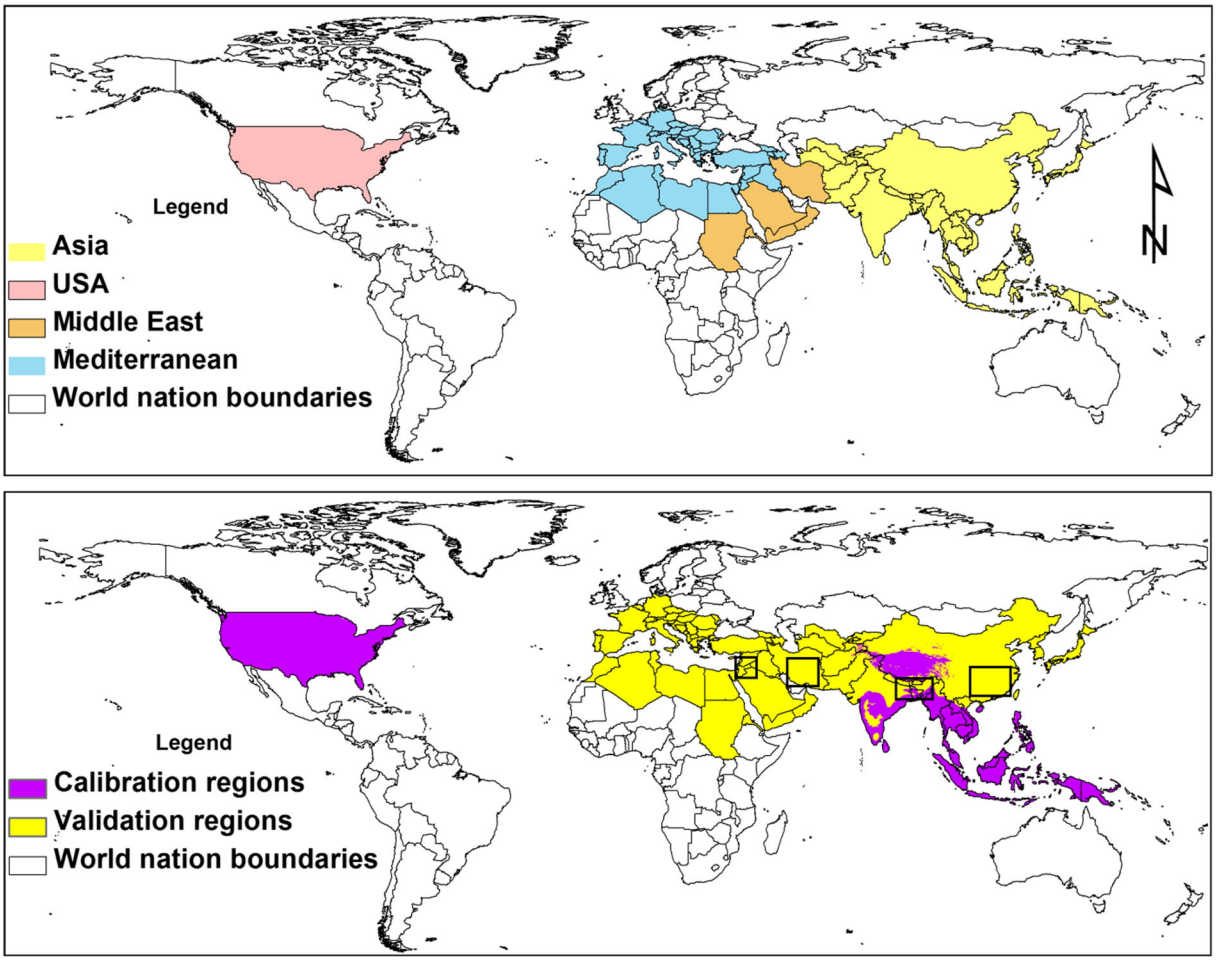

Fig. 1. Four selected global regions for estimation of error variance using regression model (the top panel) and regions selected for model calibration and validation (the lower panel). For Asia and Middle East regions, the model validation was applied only to specific regions where a good density of rain gauge stations existed (as shown in black box).

However, unlike geostationary satellites, low orbiting satellites do not provide the benefit of continuous coverage. As a result, geostationary IR estimates are used to propagate the PMW estimates at times and locations where PMW estimates are unavailable (Joyce et al., 2004). This product is also available with global coverage between 60° N and 60° S latitude at 0.25° spatial resolution for every 3 h interval.

High resolution PERSIANN-CCS precipitation product (at spatial resolution of 0.04°) is designed to fulfill the demand of hydrologist for high resolution satellite estimates in hydrologic modeling applications. The algorithm extracts different cloud features such as brightness temperature, geometry and texture of cloud patches from IR imagery and generates relationship between cloud top temperature and precipitation rate for the identified cloud patches (Hong et al., 2004; Hsu et al., 2007). Artificial neural network (ANN) approach is applied to IR estimates to generate the precipitation rate. PERSIANN-CCS has a coverage between 60° N and 60° S latitude.

For proper calibration of error variance regression model, quality validation/reference precipitation data are required.

Table 1
Summary of validation/reference data set for the study regions.

Study region	Reference dataset	Full name	Spatial resolution	Temporal resolution	Reference
The contiguous United States (area 10.5 M km^2)	NEXRAD-IV	Next-Generation Weather Radar — stage IV	0.04°	Hourly	Lin and Mitchell (2005); Fulton et al. (1998)
Monsoon Asia (area 28.5 M km^2) Middle East (area 8.1 M km^2)	APHRODITE (version: v1101)	Asian Precipitation — Highly-Resolved Observational Data Integration Towards Evaluation of Water Resources	0.25°	Daily	Yatagai et al. (2012)
Mediterranean region (area 11.6 M km^2)	ECAD E-OBS	European Climate Assessment Dataset ENSEMBLES Observational gridded data	0.25°	Daily	Haylock et al. (2008)

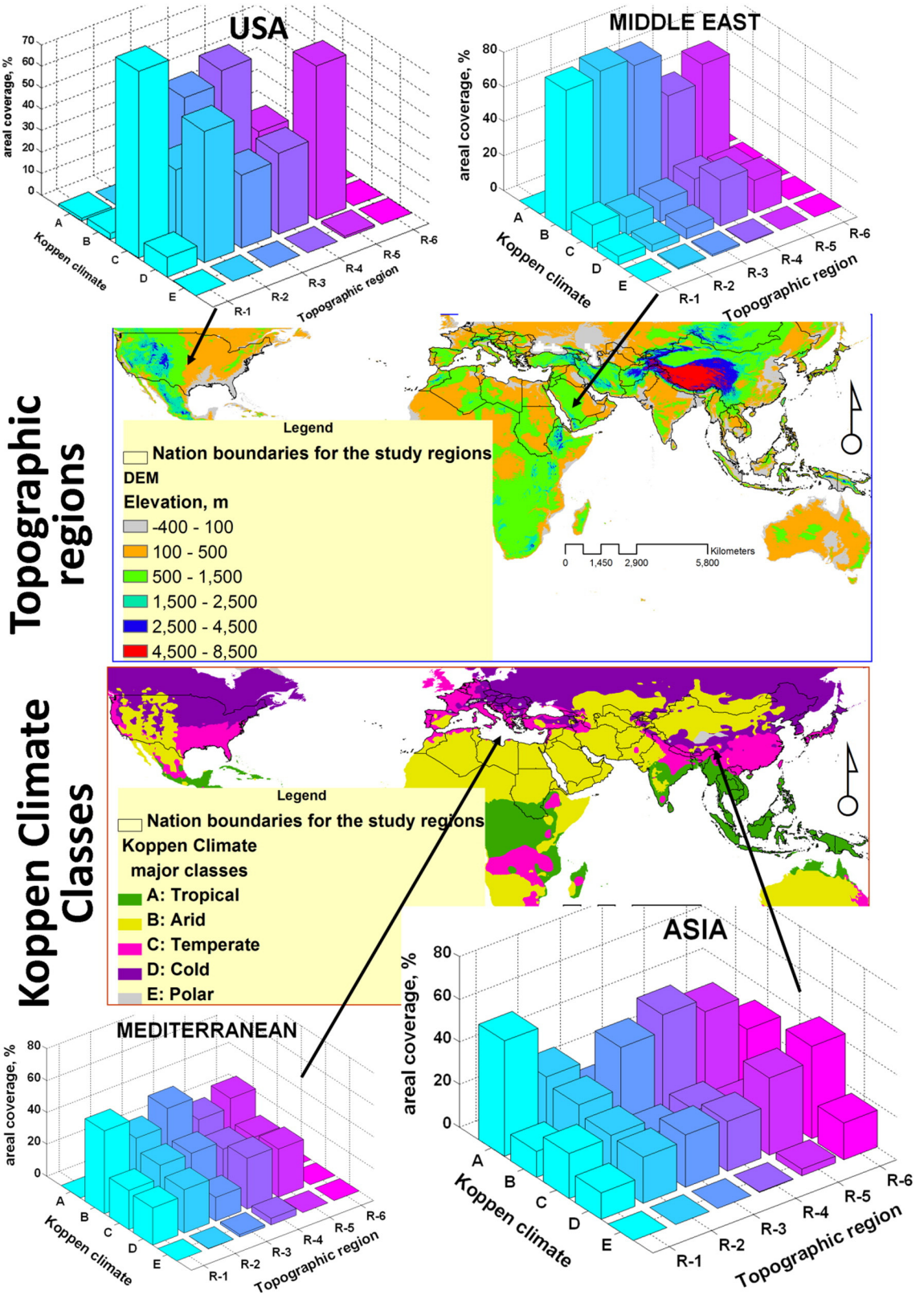

Fig. 2. Geophysical features (topographic and Köppen climate types) for the study regions and the distribution and percentage of areal coverage of these features for each region. The regions name R-1 through R-6 correspond to the topographic region mentioned in Table 2 or given in the middle panel of this figure.

Table 2
Description of topography classes, Köppen climate, and seasons.

Topographic class	Köppen climate type	Season
R-1:—400–100 m R-2: 100–500 m R-3: 500–1500 m R-4: 1500–2500 m R-5: 2500–4500 m R-6:4500–8500 m	A: Tropical (Rainforest, Monsoon, Savannah) B: Arid (Desert, Steppe, Hot, Cold) C: Temperate (dry summer & winter, hot, warm & cold summer) D: Cold (dry summer & winter, hot, warm & cold summer, very cold winter) E: Polar (Tundra & Frost)	1: Winter (Dec, Jan, Feb) 2: Spring (Mar, Apr, May) 3: Summer (Jun, Jul, Aug) 4: Fall (Sep, Oct, Nov)

Various reference datasets are considered for each study region as presented in Table 1. As quality control measures, all reference data have been assessed against available ground stations, CPC-Unified and 2A25-PR (TRMM Precipitation Radar) datasets. A point to note is that this step is only a QA/QC exercise to gauge if the selected gridded datasets can be used for calibration and validation of the error variance model. The CPC or the PR2A25 was not used in the actual calibration or validation of the error variance model. Station precipitation records from Asian Precipitation — Highly-Resolved Observational Data Integration Towards Evaluation of Water Resources (APHRODITE, Yatagai et al., 2012) represented a key source for ground data for Asian regions. Additional station precipitation records from the Bangladesh Meteorological Department, Nepal Department of Hydrology and Meteorology, Pakistan Meteorological Department, European Climate Assessment & Dataset (ECAD), and National Oceanic and Atmospheric Administration (NOAA) were used to check the consistency of the reference datasets. The CPC Unified dataset is a gauge-based gridded precipitation using optimal interpolation (OI) objective analysis technique at 0.5° spatial resolution from over 30,000 stations globally (Xie et al., 2007; Chen et al., 2008). The 2A25-PR is TRMM's high resolution orbital radar data which provides the three-dimensional storm structures both over the ocean and land surfaces (Iguchi et al., 2000).

Fig. 3 presents Quality Assessment and Quality Control (QA/QC) for APHRODITE and ECAD E-OBS datasets over Asia and Mediterranean regions. Closer inspection revealed that similar spatial precipitation distribution was observed by APHRODITE, CPC-Unified, and 2A25 PR precipitation estimation for three randomly selected days (Fig. 3, left-top). In addition, error metrics analysis and scatter plot correlation were performed. The error metrics analysis involved: 1) Frequency Bias, FB (ideal value = 1); 2) False Alarm Ratio, FAR (ideal = 0, worst = 1); 3) Probability of Detection, POD (ideal = 1, worst = 0); 4) Hit Rate, HR (ideal = 1, worst = 0); 5) Threat score, TS (ideal = 1, worst = 0); and 6) Root Mean Square Error, RMSE. In this study, 0.1 mm/day of threshold value was

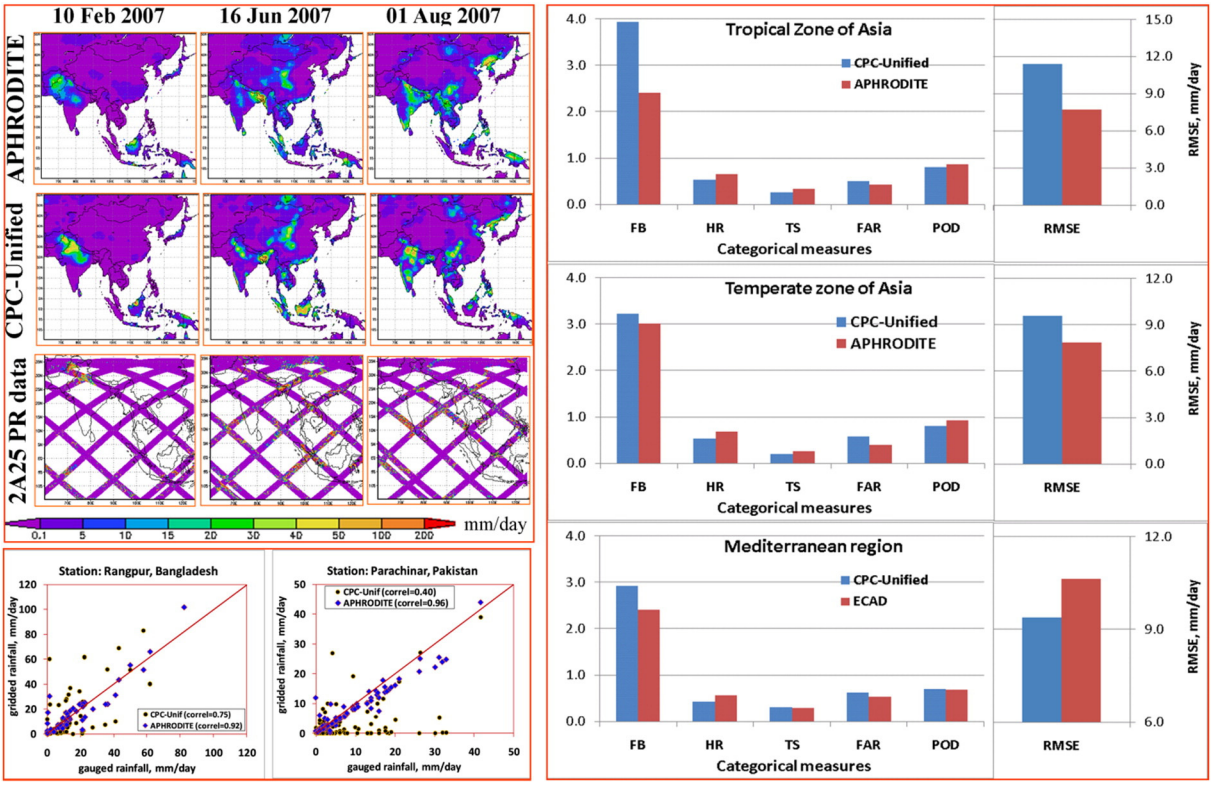

Fig. 3. Quality Assessment and Quality Control (QA/QC) for APHRODITE and ECAD datasets over Asia and Mediterranean regions. Upper left panel — spatial comparison of APHRODITE, CPC-Unified and 2A25 PR rainfall data for three randomly selected days; Upper lower panel — scatter plot of two gauging stations in Asia with APHRODITE (blue mark) and CPC-Unified (black mark); Different error metrics (FB: False Bias, HR: Hit Rate; TS: Threat Score, FAR: False Alarm Ratio, POD: Probability of Detection; and RMSE: Root Mean Square Error) for APHRODITE and CPC-Unified products in Asia and Mediterranean regions. (For interpretation of the references to colour in this figure legend, the reader is referred to the web version of this article.)

used for precipitation–no precipitation condition (Tian et al., 2009).

For Asia region, the analysis was done by dividing the region into two parts: the tropical zone (approximately bound by 23.4378° N and S) and the temperate region (above 23.4378° N). Both datasets exhibit high POD value (above 0.8) and moderate FAR (around 0.5). This shows that the precipitation events during the selected three days are detected well by both datasets. However the FAR is moderately high showing that both datasets reveal false rain detection during these particular periods. In general, based on a combined assessment of RMSE and categorical measures, APHRODITE datasets were found to be more accurate than CPC-Unified. Based on RMSE alone, CPC-Unified was found more accurate than ECAD. However, for categorical measure, the case was vice versa. Due to the fact that ECAD is available at higher resolution (0.25°) than CPC-Unified (0.5°), ECAD was selected as the appropriate reference dataset for this study. The correlation between two stations (Rangpur in Bangladesh; Parachinar, in Pakistan) and the reference datasets is demonstrated using scatter plots. As seen in Fig. 3 left-bottom, APHRODITE data is strongly correlated with the gauge records at both stations.

In general, APHRODITE data has used extensive gauges from various partner organizations more than the CPC-Unified. The number of stations incorporated in the gridding process ranged from 5000 to 12,000, representing 2.3 to 4.5 times the data available through the Global Telecommunication System network, which were used for most daily grid precipitation products. All the gauges used in CPC-Unified have been included in APHRODITE. Moreover, in case of APHRODITE dataset, extensive quality control procedure has been applied manually before the gridding procedures apply (Yatagai et al., 2012). Therefore, all these factors likely contribute to the acceptable quality of the APHRODITE dataset. For the purpose of comparing the performance of each satellite precipitation product, it is important to avoid the spatio-temporal scale differences among them. As a result, there is a need to conduct the study at a consistent spatiotemporal scale (at 0.25° and daily spatial and temporal scales, respectively). This is done by aggregating those products which are available at finer scales, such as PRESIANN-CCS, NEXRAD-IV in 0.04° spatial scales, NEXRAD-IV in hourly temporal scale, and 3B42RT and CMORPH in 3-hourly temporal scales.

2.3. Methodology

For estimation of error variance, a nonlinear regression model framework is developed for the contiguous United States and Monsoon Asia regions. The satellite precipitation rate and error variance are used as independent and dependent variables, respectively. Prior to fitting the model, the observed error variance and precipitation rate are segregated into various regions based on topography, climate, and season types (detailed description is provided in Gebregiorgis and Hossain (2013a)). For each regions, the model estimators (α and β) are then determined. The key assumption here is, for similar topography and climate in the validation regions (Mediterranean, Middle East), the estimators remain similar with the estimators from calibration regions (USA and Asia). Accordingly, the error variance was simulated for all study regions using Eq. (1).

Moreover, error characterization is an important task to evaluate the performance of regression model. Since satellite precipitation rate is the only independent variable in the regression model framework, it produces zero error variance when the satellite precipitation products miss a rain event on the ground in certain location. For a particular product and region where missed precipitation is dominant, the accuracy of error variance is therefore not reliable. Therefore, to understand the nature of the error, the total bias of the three satellite precipitation products was decomposed into hit, miss-rain, and false-rain biases (Tian et al., 2009) for each region at daily time scale and then converted to seasonal average.

The detailed mathematical formulation used in the error decomposition scheme is presented in Tian et al. (2009). Let P_s and P_g be the precipitation from satellite estimate and ground truth, respectively. The binary-valued precipitation event mask, K, is derived based on the magnitude of the precipitation estimate (1 if $P > 0$ and 0 if $P = 0$). The error components' mask can be defined based on Eqs. (2)–(8) as follows:

$$\text{Hit mask}, K^H = K_s \times K_g \tag{2}$$

$$\text{Miss mask}, K^M = K_g \times K_s' \tag{3}$$

$$\text{False mask}, K^F = K_s \times K_g' \tag{4}$$

where K' denotes the Boolean complement of the binary mask K. If E is the total error, H is the hit bias, M is miss-rain bias, and F is false-rain bias, then

$$E = P_s - P_g \tag{5}$$

$$H = \left(P_s - P_g\right) \times K^H \tag{6}$$

$$M = P_g \times K^M \tag{7}$$

$$F = P_s \times K^F. \tag{8}$$

To evaluate the performance of the regression model during the calibration and validation periods, various metrics such as coefficient of correlation (r), covariance (cov), Standard Error of Estimates (SEE), Nash–Sutcliffe efficiency, E (Nash and Sutcliffe, 1970), and index of agreement, d (Willmot, 1981) are used. The mathematical equations of these performance measures are presented in Appendix A.

3. Discussion of result

3.1. Error characterization

In this paper, we only presented the characteristics of error component of Asian region for the winter and summer seasons. To provide our readers with the complete picture of the error characteristics, we provided additional explanation about the

nature of the error components of other study regions without any quantitative and qualitative results at the end of this section. Fig. 4 presents the error components of the three satellite precipitation products over Asian region for the winter (upper panel, three rows) and summer (lower panel, three rows) seasons. The three products, shown in Fig. 4, share one similar feature in common. For all products, the dominant source of total bias for the southern tropical region (around equator) is positive hit bias. This shows that all satellite precipitation algorithms have the ability to detect the equatorial heavy precipitation at the screening stage but they overestimate the rain rate at the retrieval stage. For the winter season, the northern part of Asia (temperate region) is mainly characterized by negative and high positive total bias for CMORPH and PERSIANN-CCS products, respectively. In case of PERSIANN-CCS, the substantial positive total bias arises from the contribution of both positive hit bias and false precipitation particularly over Himalaya region.

For the summer season, positive hit bias and missed precipitation are the major sources of the total error in case of 3B42RT over the tropical region. In fact, the miss-rain bias is more dominant over low land regions (India and Bangladesh). For CMORPH product, the contribution of both negative hit bias and missed precipitation enhances the negative total error over

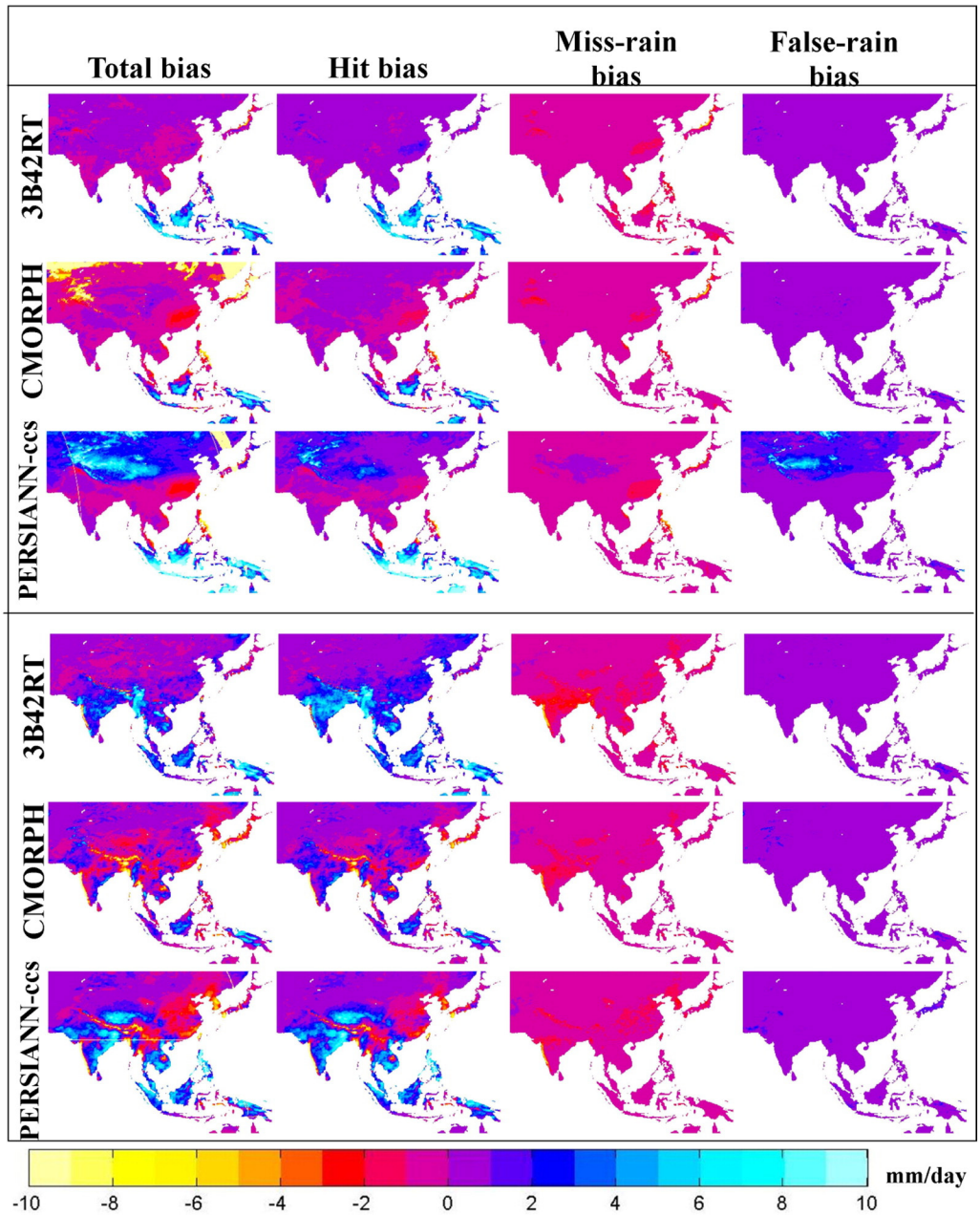

Fig. 4. Decomposition of satellite rainfall error components for Asia region during the winter (upper panel, three rows) and summer (lower panel, three rows) seasons of 2006–2007.

the Himalaya and Bangladesh regions. For PERSIANN-CCS, the missed precipitation is relatively low as compared to CMORPH and 3B42RT products.

In general, the dominancy of error components varies from location to location for the three satellite rainfall products. For instance, for snow season, missed precipitation is the dominant error component almost for the three satellite rainfall products: e.g. for northeast of USA during the winter season, for Himalaya region during spring and summer seasons, the missed precipitation is significant as compared to the other seasons. This could be related to the inability of satellite sensors to detect rain drops over snow cover areas (Tian et al., 2009; Gebregiorgis et al., 2012). However in most cases, hit and false precipitation bias are the major error components for most of the regions. False bias for PERSIANN in Asia region, false and hit bias for CMORPH product in Middle East region are some of the examples. As a summary, hit bias is the major error component for all products in all regions during the rainy seasons.

3.2. Model estimators

The model estimators, computed from the observed error variance and satellite precipitation rate, were compared for regions of similar topography, climate and season. According to the hypothesis of this study, error information can be transferable from one location to another provided that the regions have similar topographic and climate features and seasons. In other words, the regression equations developed on the calibration regions (USA and part of Asia) were used to estimate the error variance on the other part of the regions provided that the aforementioned governing factors are similar. Therefore, in these regions, the regression estimators need to be comparable.

Fig. 5 shows the model estimators (α and β) for 3B42RT product over the study regions. First, the estimator α is relatively comparable for most of the regions. However, α value shows significant discrepancy for lowland (R-1) and cold regions (D/1, 2, 3, 4; see Table 2 for the nomenclature). The estimator α is very high for USA and very low for Middle East (See Fig. 5, first row), particularly for the winter and spring seasons (D/1, 2). In case of USA, these regions specifically represent the northeast coastal regions. For the same regions, the estimator β is very low for USA and high for the remaining three regions. Despite the similarity of topography and climate, we speculate that the reason for the inconsistency of α and β in these regions is mostly linked to the presence of snow cover in the northeast coastal region of USA during the winter and spring seasons. As a result, the error variance curves in these regions have different rates of growth and shape. For the case of USA, the error variance is not highly sensitive to precipitation rate as it does for the remaining three regions during the winter and spring seasons. In general, in addition to topography, climate and season, geographical proximity is also an important factor that needs to be considered during the transfer of model estimators from gauged to ungauged regions. The closer the regions, the similar estimators they are expected to have. In this article, we only present the estimator for 3B42RT as a representative example. Like 3B42RT, the estimators for CMORPH also reveal similar features. For PERSIANN-CCS product, the estimator variation is not only limited to lowland and cold climate but also extends to lowland and temperate climate regions.

3.3. The measures of multiple correlative associations

The performance of error variance regression model is tested using the measures of multiple correlative associations between the observed and predicted error variance. These include the multiple correlation coefficient (R) corrected for $n - 1^{\circ}$ of freedom where n is the size of data sample (from 2003 to 2005, $n = 1096$) and the unbiased Standard Error of Estimates (SEE). These have been done by aggregating the observed and predicted error variances of individual pixels over each region at a daily time step. As seen in Fig. 6 (upper panel), the multiple correlation coefficients show strong association between the observed and predicted error variances in most of the regions for 3B42RT product. However, there are some offbeat situations where R is very small in the calibration and validation regions (USA and Mediterranean regions). These locations are highland and arid climate regions of USA during the summer and fall seasons (R-5/B/3 and R-5/B/4, respectively) and Mediterranean regions during the summer season (R-5/B/3). The poor predictive performance of the model in these two particular regions could be related to the presence of missed precipitation or/and the quality of the reference data in the regions. For 3B42RT product missed precipitation is a common problem over mountainous regions, such as Rockies during the winter season not during summer and fall (Tian et al., 2009; Gebregiorgis et al., 2012). On the other hand, the western and northwestern highlands of USA are known to be poorly covered by radar and gauges (Maddox et al, 2002). Hence, the quality of NEXRAD IV data is a potential reason for the poor performance of the model.

The Standard Error of Estimates is a measure of the accuracy of predictions made with a regression model. It is computed as the square root of the average squared error of the predictions. Thus, the smaller the SEE, the better the prediction of the model. Fig. 6 (lower panel) shows the SEE between observed and predicted error variances of 3B42RT product. For the same reason mentioned in the previous paragraph, the SEE of 3B42RT is high over the highland and arid regions of USA during all seasons. In general, both the correlation and SEE reveal the good performance of the error variance model in the remaining regions.

3.4. Error variance estimation

The regression model was implemented to estimate the error variance of the three satellite precipitation products at a daily time scale. Fig. 7 presents the simulated, observed, and residual error variances, and ratio of computed error variance to ground precipitation over Asia region on 03 July 2007. Along with the accuracy of the simulated error variance, the model generally captured the overall spatial pattern of the observed error variance over the region. In temperate climate region, the residual error is significantly high for the three satellite precipitation products. This shows that the model overestimates the error variance along the foothills of the Himalayan Mountains starting from the border of Pakistan all the way to Myanmar. This region is dominated by positive hit bias for 3B42RT and PERSIANN-CCS products during the summer;

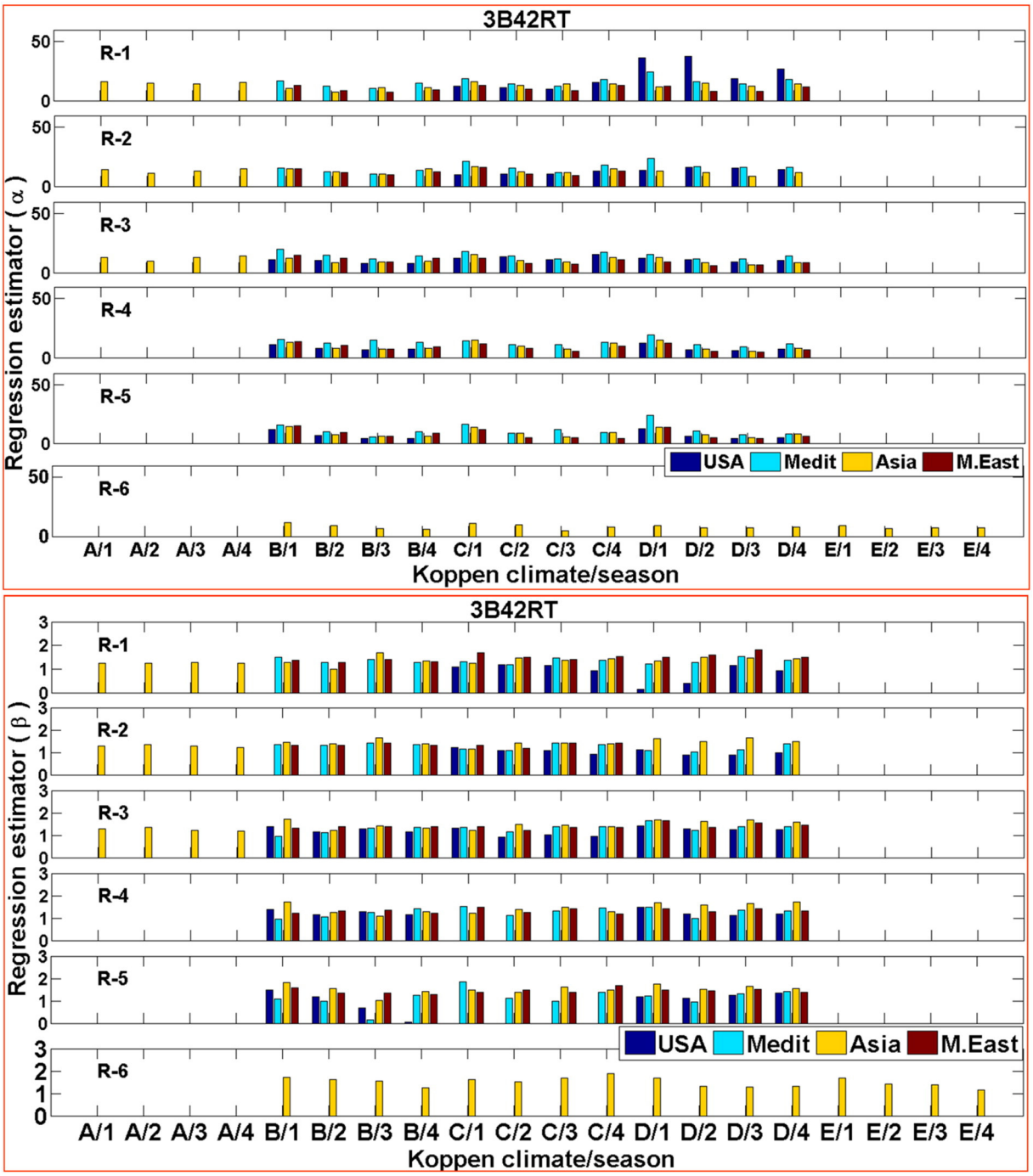

Fig. 5. Error variance regression model estimators (α and β) of the study regions for each topographic, Köppen climate class and season during the calibration period (2003–2005). The name on x-axis is designation based on Table 2.

whereas CMORPH is mainly characterized by negative hit bias particularly in northwest India and Bangladesh region. As a result of the hit bias, the model tends to overestimate the error variance in this region.

The tropical region of Asia is characterized by low residual error enlightening the good performance of the model in this region. The model also estimated well the error variance in the northern part of Asia. In fact, these regions were also characterized by small total bias due to low precipitation in the region. The map of ratio of simulated error variance to ground precipitation shows the presence of observed precipitation during that particular day. Overall, the regression model performed well in simulating the error variance over the entire region at the time of rain event.

Fig. 8 shows the simulated, observed, and residual error variances over the contiguous United States on 06 July 2006.

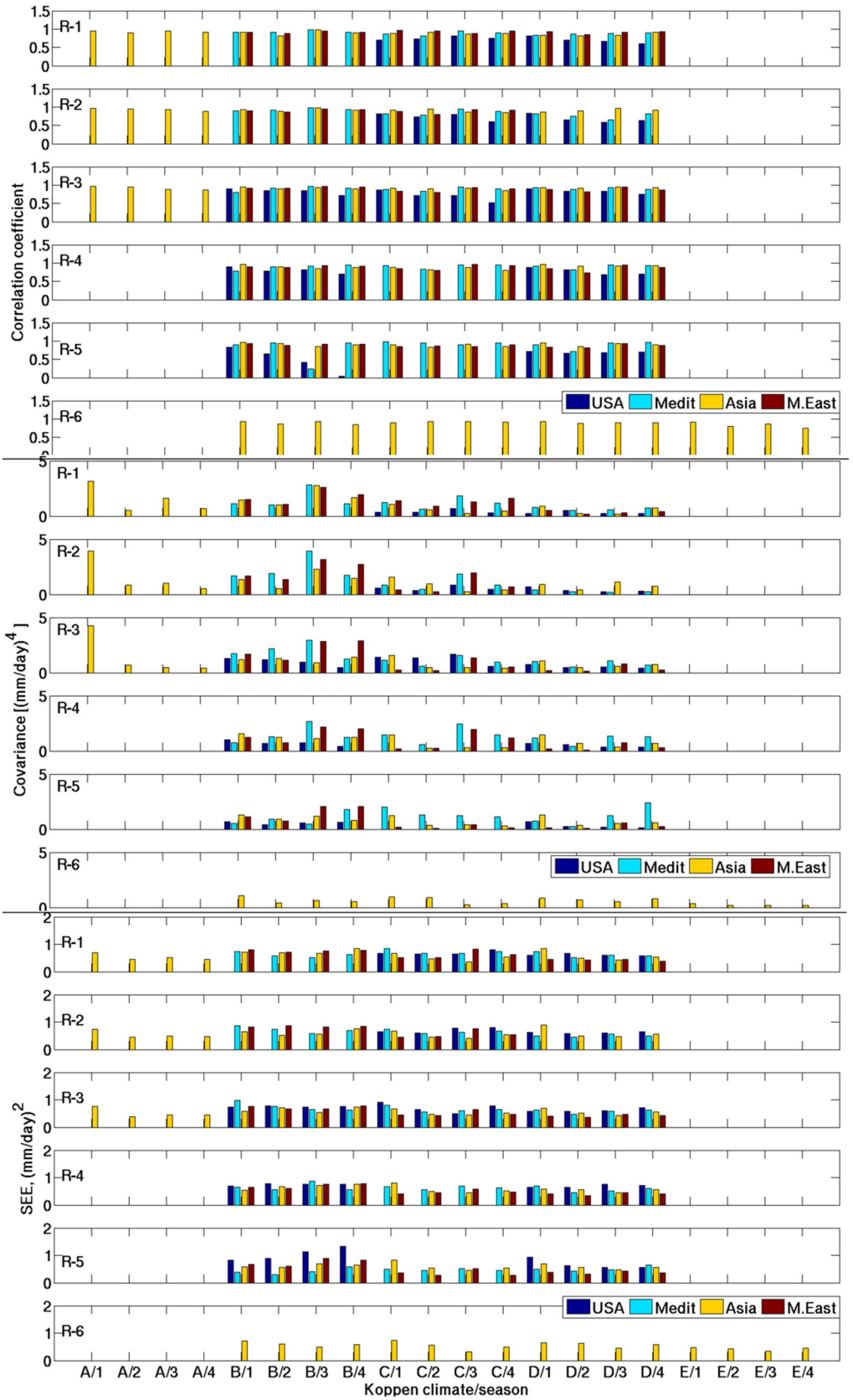

Fig. 6. Correlation (upper panel) and Standard Error of Estimates, SEE (lower panel) for observed and simulated error variance during the calibration period (2003–2005) for 3B42RT product.

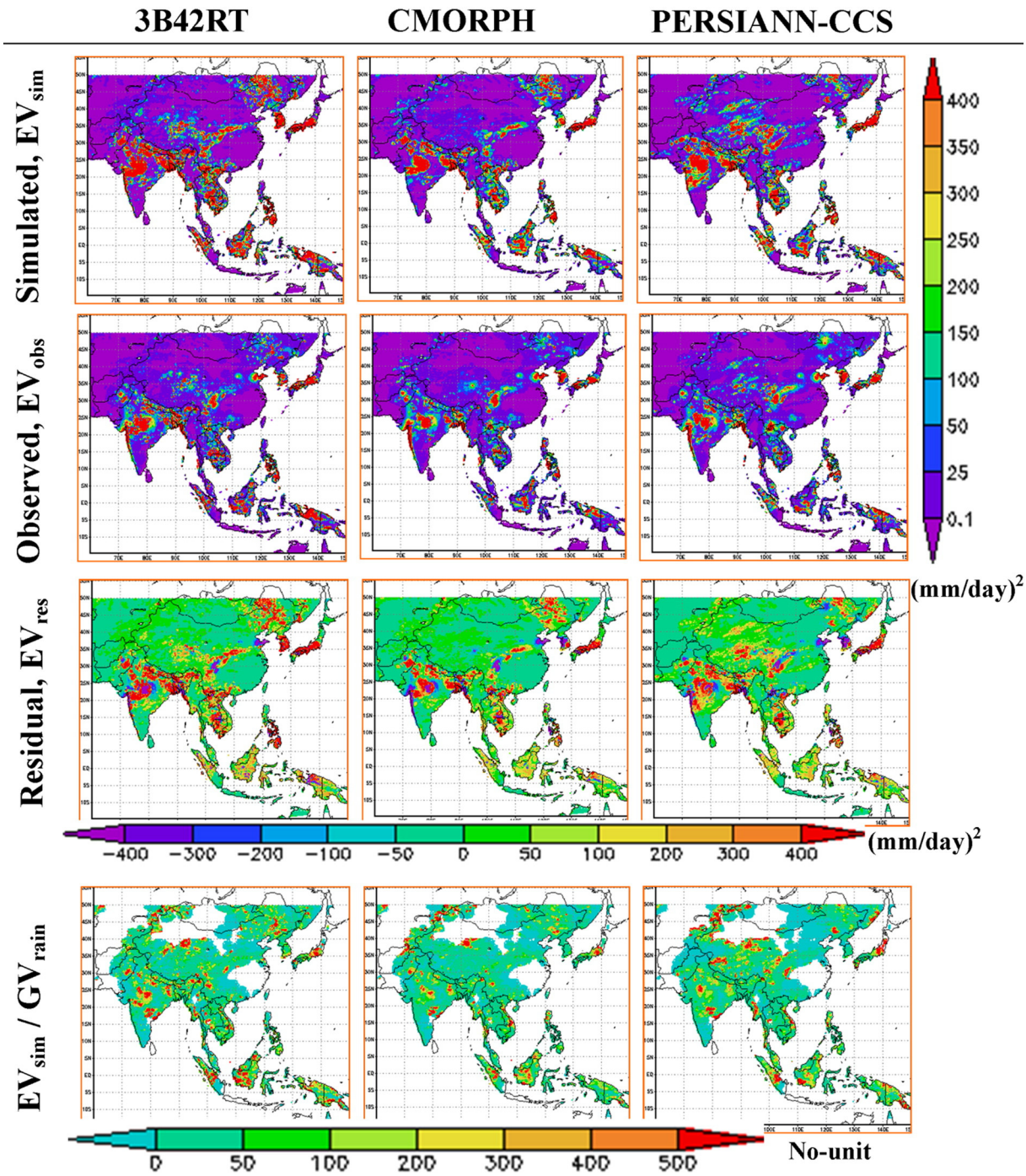

Fig. 7. Simulated, observed error variance (the first two rows panels), and residual error variance (third row), and ratio of simulated error variance to observed rainfall (bottom row) for the three satellite rainfall products over Asia region on 07/03/2007.

The three products share similarities that the simulated error variance captures the spatial distribution of the observed error variance. But in terms of prediction accuracy, the model performed well in 3B42RT and CMORPH products; whereas it over predicted in the northern part of New Mexico and Texas states and under predicted in the east coast of CONUS for PERSIANN-CCS. In the case of Mediterranean region, over small rainy region, the model overestimated the error variance for 3B42RT and CMORPH products; whereas it underestimated for PERSIANN-CCS product due to missed precipitation error (Fig. 9). For 3B42RT and CMORPH, the spatial distributions of the observed and estimated error variances were also found to be similar. The region is fully characterized by temperate (northern part) and arid (southern part) climate.

For Middle East region, model simulated error variance represents the observed error variance very well for all satellite

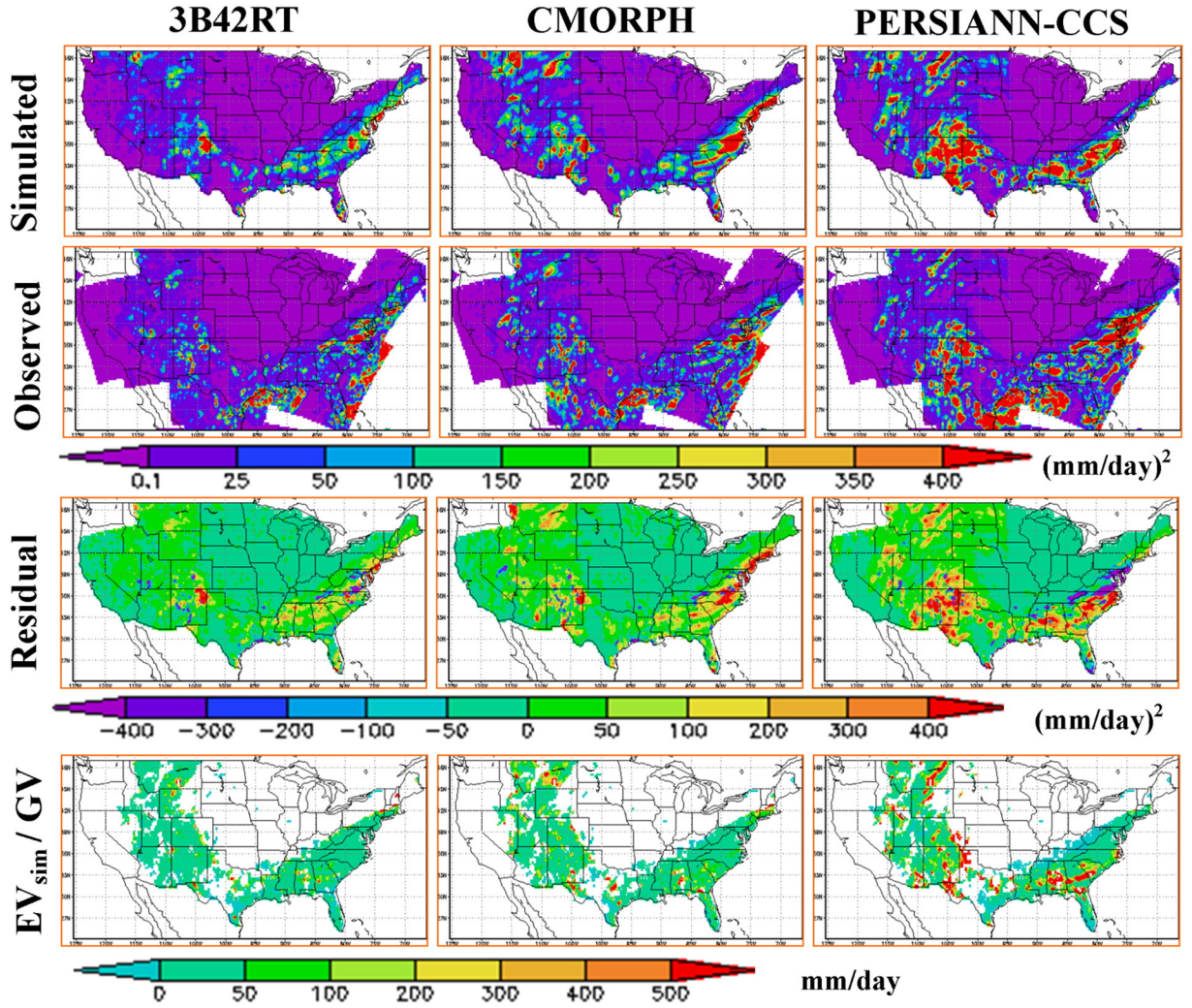

Fig. 8. Same as Fig. 7, except over USA on 07/06/2006.

precipitation products both in terms of spatial distribution and magnitude (Fig. 10). The residual error was small, particularly for CMORPH product. The PERSIANN-CCS underestimated the error variance in the eastern part of the region. This region is characterized by a single arid climate type. To summarize, the performance of the regression model has the tendency to overestimate the error variance for 3B42RT and CMORPH products in all study regions. But that is not the case in PERSIANN-CCS; it over predicts in USA for arid climate and underestimates in USA for cool climate, in Mediterranean for temperate region and in Middle East for arid climate conditions.

To see the entire nature of the error variance, the temporal trend at daily time scale was investigated by averaging spatially over each selected study region during the period of 2005–2007. Fig. 11 shows the spatial average of observed and simulated error variance for USA (top, left), Mediterranean region (top, right), East Tibet and Himalayas region in Asia (middle and bottom, left), and South Iran, Jordan and Israel from Middle East (middle and bottom, right). The model displays good performance in simulating the temporal variation of the error variance for the three satellite precipitation products during the entire period of analysis. It adequately captures the time series of error variance over the selected six regions. The model performance was found to decline for 3B42RT product over Mediterranean and Middle East regions. In case of CMORPH, the model over predicted the error variance over USA and East Tibet during the summer season (between June and August). Good performance was observed for CMORPH over Mediterranean, south Himalayas in Asia, and Jordan and Israel in Middle East regions. For PERSIANN-CCS, the model overestimated the error variance in USA during the whole seasons except between September and November (fall season). However, it also exhibited improved performance in the validation regions of Asia and Middle East.

In summary, for time series error variance, the efficiency of the model was assessed by three performance measures: coefficient of correlation (r), Nash–Sutcliffe efficiency, E (Nash and Sutcliffe, 1970), and index of agreement, d (Willmot, 1981). The correlation coefficients in most cases were above 0.6 except for two regions (Mediterranean and Middle East–south Iran region) that yielded 0.48 and 0.56 for PERSIANN-CCS and CMORPH products, respectively (Fig. 12, top panel). The nearest

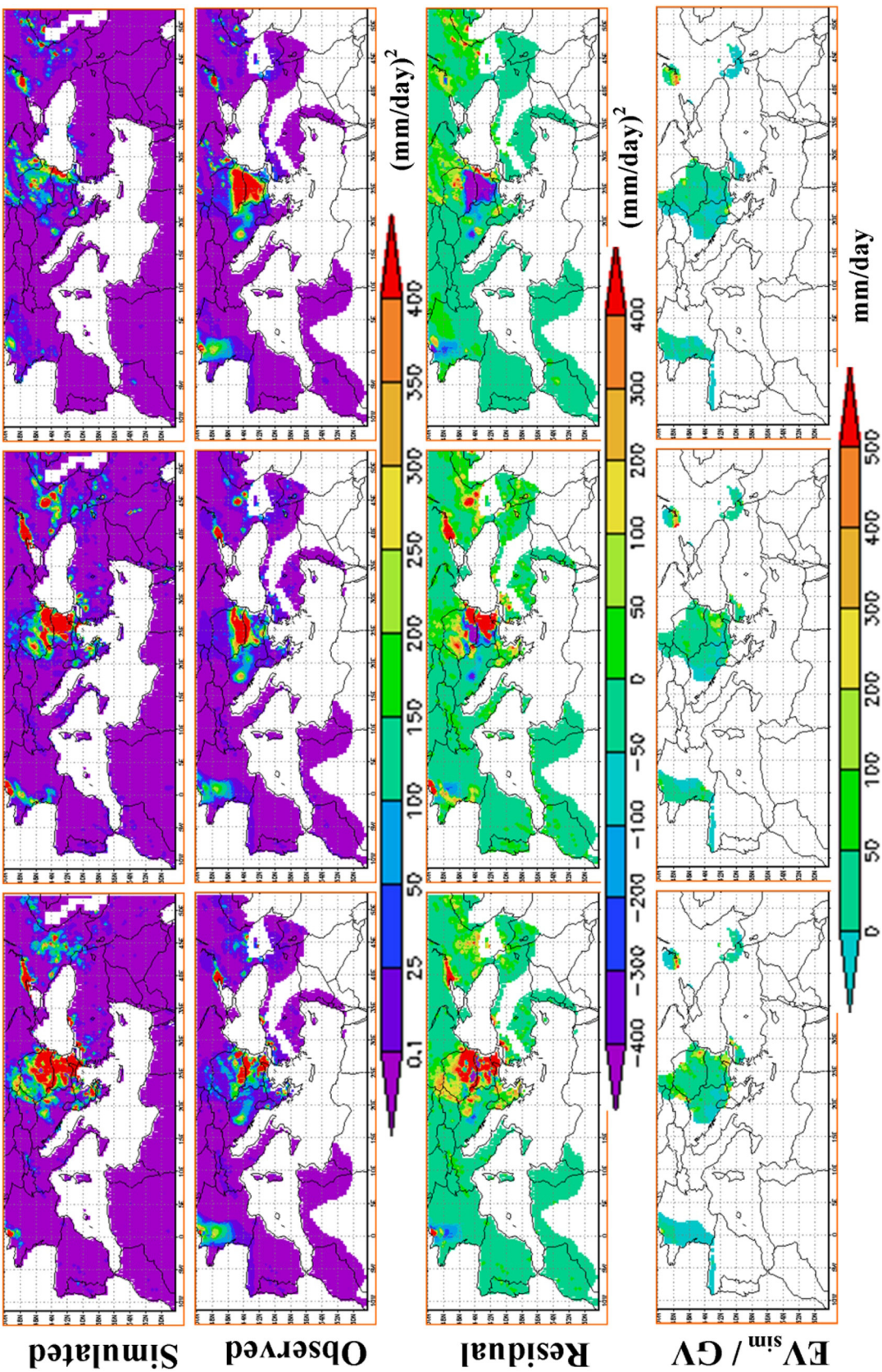

Fig. 9. Same as Fig. 7, except over Mediterranean region on 06/18/2007.

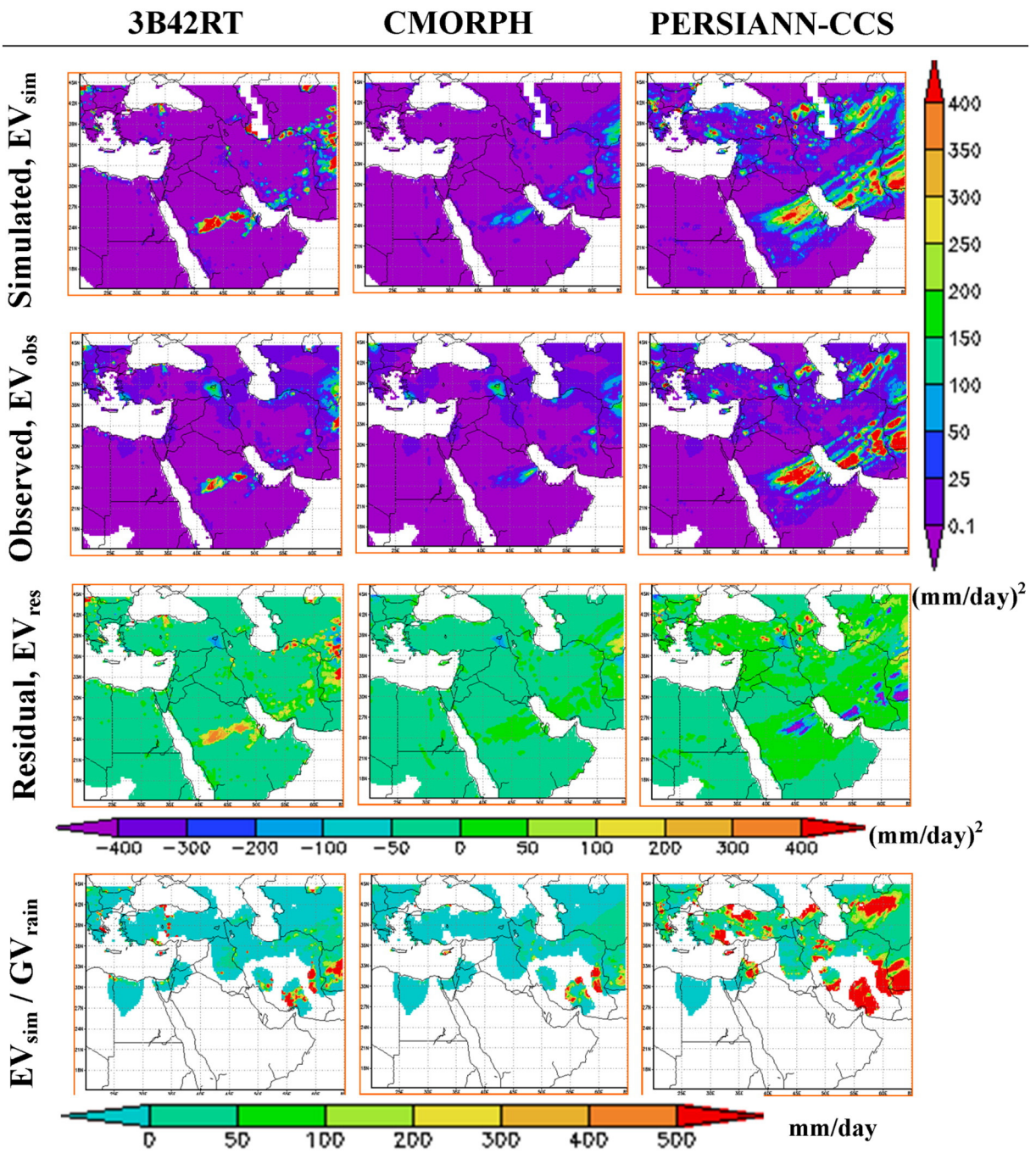

Fig. 10. Same as Fig. 7, except over Middle East on 02/17/2006.

r value to one means, the smallest dispersion of the predicted error variance to that of the observation. This shows that the dynamics of the observed error variance trend is captured very well by the model even though it exhibits strong biases, which in some regions is much higher than the actual variability of the error.

Based on Nash–Sutcliffe efficiency (Fig. 12, middle panel), the error variance model showed poor prediction over Mediterranean region for 3B42RT and PERSIANN-CCS products, respectively. The range of E lies between 1 (ideal value) and −∞. Negative efficiency indicates that the mean value of the observed error variance would have been a better predictor than the model. In fact, one of the major problems of Nash–Sutcliffe efficiency, since it squares the difference between the observed and predicted error variances, is that the efficiency can be exaggerated with the presence of high prediction in the time series (Legates and McCabe, 1999). On the contrary, it is insensitive for small differences between observed and

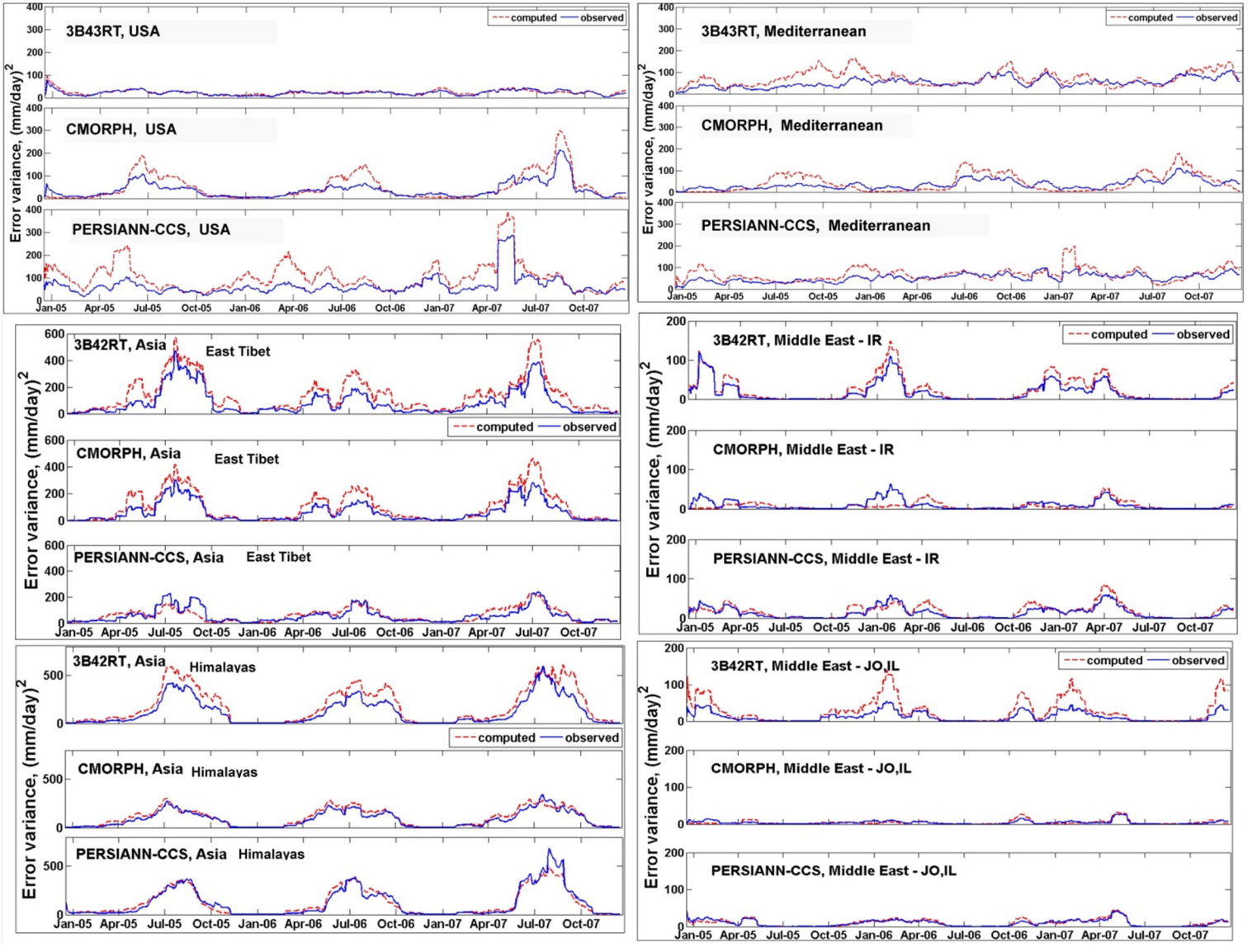

Fig. 11. Temporal trend of observed and simulated error variances of the three satellite rainfall products over the study regions for the period of 2005–2007. To avoid visual cluttering, a 31 day moving average is applied. For Asia and Middle East regions, the spatial average was performed only for selected four sub-regions: East Tibet, Himalayas, Iran (IR), Jordan (JO), and Israel (IL). Refer to Fig. 1, lower panel for locations.

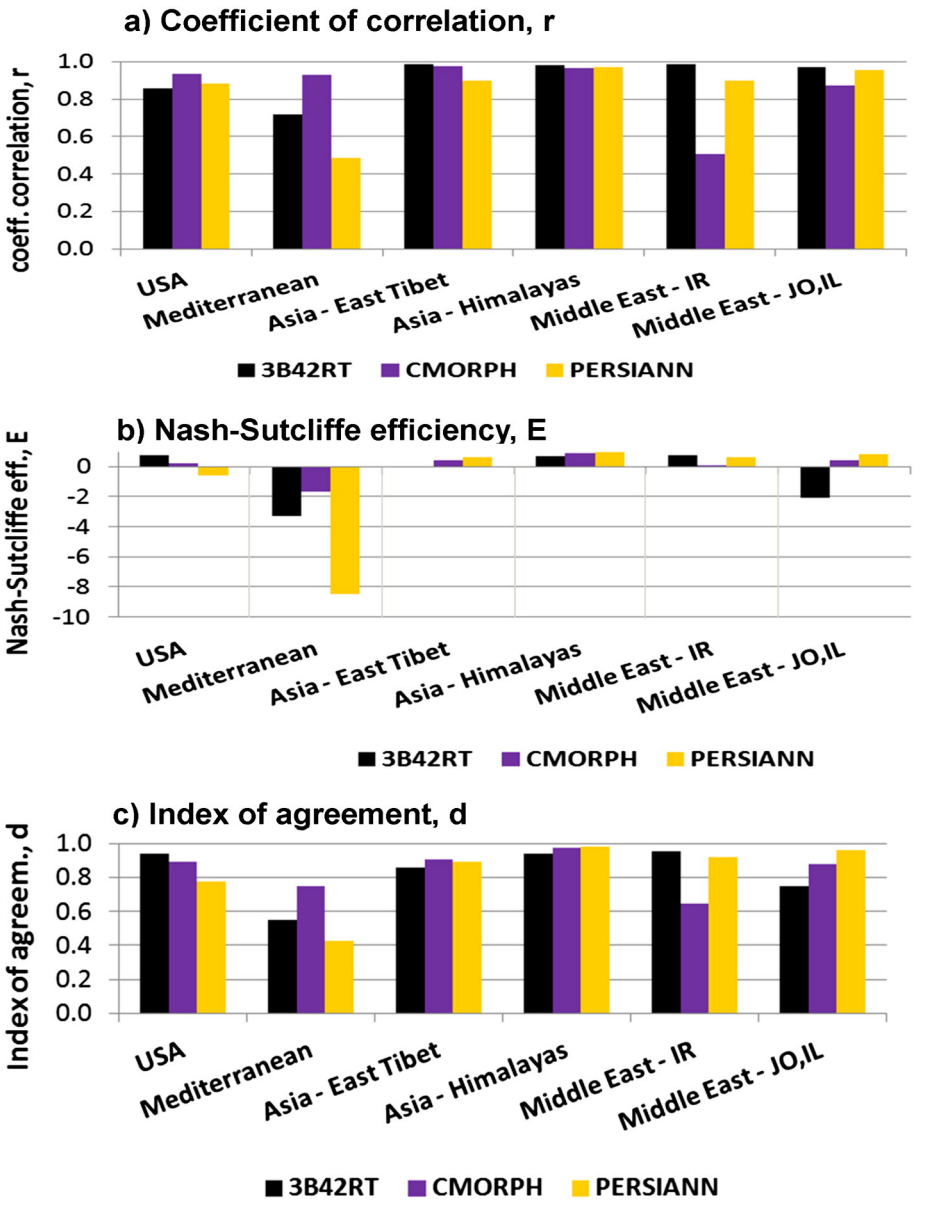

Fig. 12. Correlation coefficient (top panel), Nash–Sutcliffe efficiency (middle panel), and index of agreement (lower panel) between observed and simulated error variances for all study regions (as labeled in Fig. 11) during 2006–2007.

predicted. For instance, in Mediterranean and Middle East (JO, IL) regions, the model overestimates the error variance during the winter season for PERSIANN-CCS and 3B42RT, which eventually result in high negative efficiency.

The index of agreement (d) is also computed as seen in Fig. 12, lower panel. Like coefficient of determination, r^2, the value of d ranges between 0 (no correlation) and 1 (perfect fit). This performance measure backs the results obtained from correlation coefficient. It indicates poor performance of the model in Mediterranean region for PERSIANN-CCS and 3B42RT products. In general, it can be concluded that the model predicts the error variance well in most of the regions and all products except the two cases mentioned above.

3.5. Impact of using gauged grid boxes for assessment of estimated error variance

In the above analysis (Section 3.4), the choice for our reference (ground validation) precipitation data for assessing the error variance model was gridded (spatially interpolated) datasets. Because interpolation techniques have an inherent uncertainty in interpolating precipitation over a grid box lacking in an in-situ gauge, a concern that can be raised in such an assessment is that the performance of the error variance model could lead to significantly different conclusions if restricted to grid boxes containing only in-situ gauges. Literature on the use of gridded precipitation datasets for

validation of satellite data indicates that this concern may be unfounded. In general, it is not possible to reach perfect spatial matching between point measurements from gauges and spatially averaged estimates from satellite products (Sapiano and Arkin, 2009; Romilly and Gebremichael, 2011). Fundamental difficulties exist when comparing gauge measurements

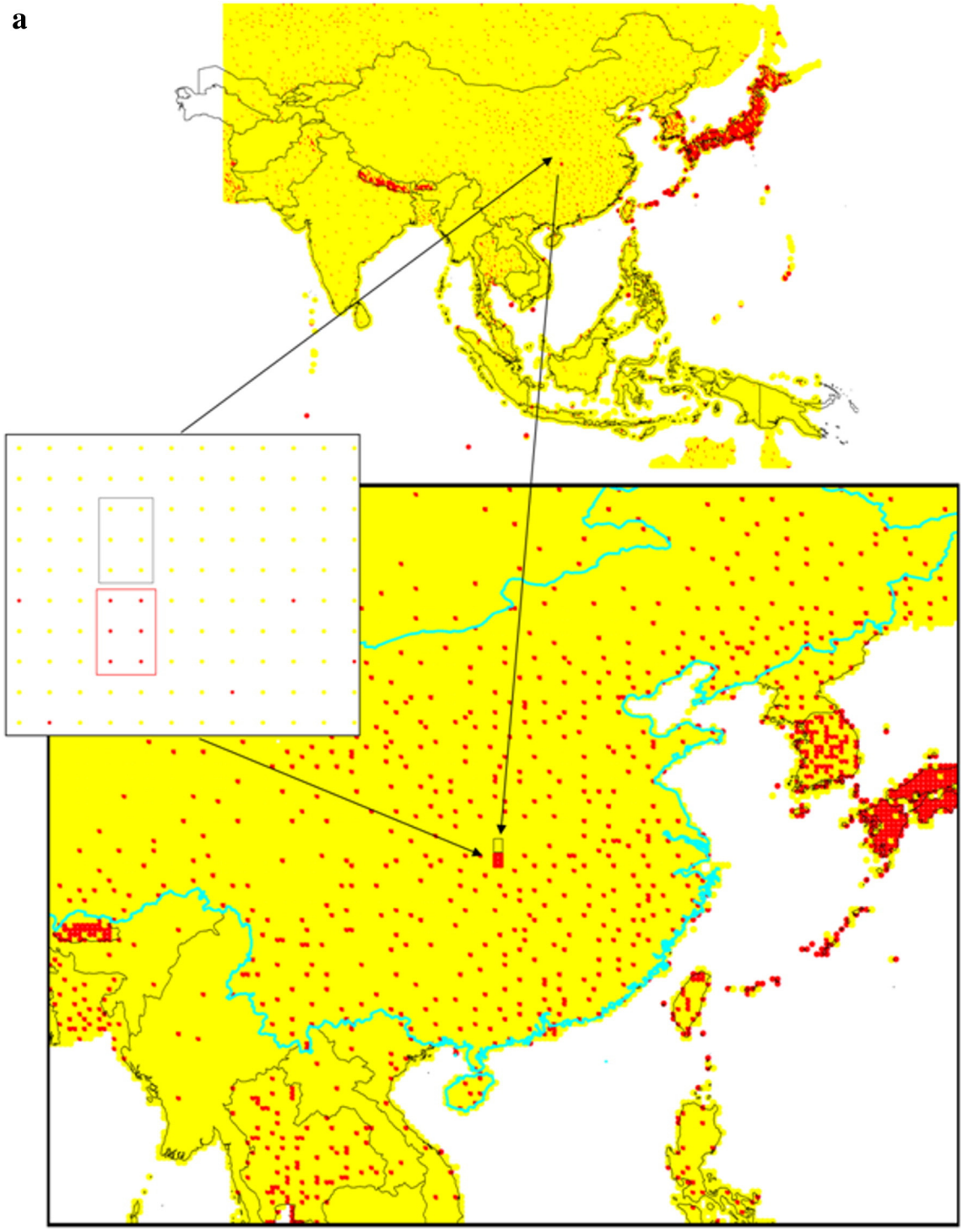

Fig. 13. a. Two 3 × 2 gridded grid boxes equipped with rain-gauge (red colour) and without rain-gauge stations (yellow colour) in East Asia region. These grid boxes were selected to test the impact of calibration and validation of the error variance model for three scenarios: a) using grid boxes with gauges; b) using only grid boxes with no gauges and c) using both gauged and ungauged grid boxes. b. The comparison of simulated error variance from three different calibration approaches using data and grid boxes from panel a: gauged-only, ungauged-only, and combined grid boxes (gauged and ungauged), shown with observed error variance at the gauged grid boxes. (For interpretation of the references to colour in this figure legend, the reader is referred to the web version of this article.)

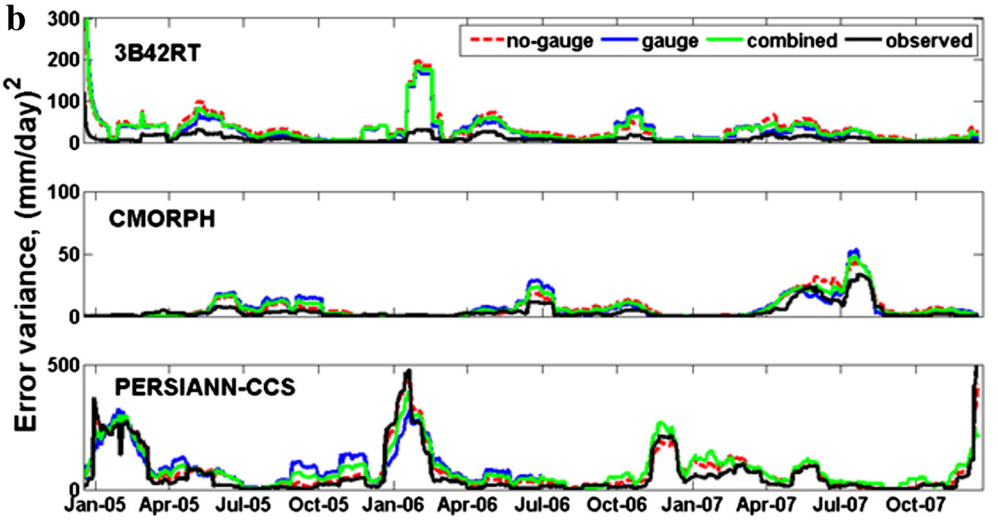

Fig. 13 (*continued.*)

and satellite estimates: retrieval errors of satellite algorithms, sampling errors caused by different sampling schemes, systematic gauge errors related to instruments, etc. (Ciach and Krajewski, 1999; Bowman, 2005). As long as a robust interpolation technique is employed in the gridding process, where the uncertainty of the interpolation is significantly smaller than the uncertainty due to sampling or retrieval (e.g. Huffman, 1997; Gebremichael et al., 2003), such gridded data can be used as ground validation as there is simply no better practical alternative (Maurer et al., 2002; Adler et al., 2003; Tong et al., 2013). A point to note here for readers is that if the error variance model development restricted itself to the use of only the grid boxes containing in-situ gauges, then a sufficient range of climate and topography (most in-situ gauges are located in lower elevations) would not be available for the calibration of the error variance model. Consequently, the error variance model would lack global value for use over the vast ungauged regions of the world.

Nevertheless, in order to provide added confidence for global applications, we have assessed the impact of the performance of the error variance model by considering calibration (and validation) for the following three scenarios: a) using only the grid boxes containing in-situ gauges; b) using only grid boxes (gridded) without in-situ gauges and c) using grid boxes that are both gauged and ungauged (the approach that we have used in our study). Fig. 13a shows two regions we have selected in East Asia comprising 3×2 0.25° grid boxes. One region of 3×2 grid boxes is entirely ungauged (shown in yellow circles), while the other is entirely gauged (shown in red circles). Fig. 13b shows the estimated error variance for the three satellite products calibrated (during the period of 2002–2005) and then validated independently (during the period of 2005–2007) for the three scenarios (gauged-only, ungauged-only and combined). It is clearly seen that restricting the calibration and validation of the error variance model to grid boxes containing only in-situ gauges has no discernible impact on the performance of the error model scheme. Careful inspection also reveals that the findings of this test are consistent with what is reported in Fig. 11 across the wider geographic region of East Asia. Therein (in Fig. 11) we observe that PERSIANN provides the most accurate estimation of error variance. This test also proves that the quality of the gridded datasets we have used for assessment of error variance is quite acceptable for drawing conclusions over a much larger area of application that is mostly ungauged.

3.6. Conclusion and recommendation

The broader impact of this study is that the global availability of error information for three satellite precipitation products can advance the operational use of satellite precipitation estimate for a wide range of applications. In particular over ungauged regions of the world, predicting satellite precipitation error information from easily available geophysical features is an alternate and pragmatic solution to perform meaningful prediction using satellite precipitation data for many applications. Just like nutrition label informs a potential consumer at a super market, we believe that satellite precipitation products should also be available to end users with essential error information associated with the products. Non-negligible and unavoidable errors inherent in satellite precipitation estimates can result in wrong applications if the errors are unknown a priori. Even though there have been several studies regarding the estimation and characterization of satellite precipitation uncertainty (e.g. Zhang et al., 2013; Gebregiorgis et al., 2012; Tian and Peters-Lidard, 2010; Hong et al., 2006; Nijssen and Lettenmaier, 2004; Hossain and Anagnostou, 2004; Huffman, 1997, among several others), an approach that explicitly integrates the estimation techniques in the absence of any reference ground data is, to our knowledge, is not yet universal.

Therefore, we propose a method of predicting satellite precipitation error variance from easily available geophysical information to users. Such a method can be practically applicable to ungauged regions of the world where satellite precipitation estimates are the only viable source for several applications including decision making. To this end, our purpose is not to provide information on which satellite product is the best, but rather to examine simplest and practical ways of knowing an a priori approximate error associated with a product from

information easily available to end-users. We believe that this kind of study is an important step forward to deal with satellite precipitation uncertainty in regions where ground validation data is absent.

Essentially, this study provides the error variance of three satellite precipitation products for satellite precipitation data users. Before using satellite precipitation estimate for specific application, understanding error information can help users to choose the appropriate product, find out the level of accuracy of their prediction, and then make meaningful prediction. Beyond that, the end user communities can also develop trust on information coming through satellite precipitation prediction. The users can build confidence to apply the data for societal benefits, as has been recently demonstrated for the case of satellite altimetry (Hossain et al., 2014). It opens up more possibilities for satellite data to intervene in day to day social activities, such as tourism, entertainment, and large social gatherings.

Our study is done not without limitations. The error variance model has a drawback in predicting the error variance in location where missed precipitation is dominant. It produces zero error variance for a single storm which is missed by satellite. It significantly underestimates the error budget accumulated over specific period (such as for daily accumulated precipitation) if missed precipitation is the major contributor to the total precipitation error. Therefore, in addition to precipitation rate, other independent variables need to be considered (such as surface temperature, lapse rate, integrated water vapour) in the regression model to avoid the dependability of error variance on precipitation alone. Moreover, implementation of advanced approach (such as probabilistic methods) is recommended to further understand the connection between geophysical features and satellite precipitation uncertainty. For instance assessing and quantifying the probability of being missed-rain, or false bias, as a function of the geophysical nature would be worthwhile. Moreover, topography, climate, and seasons are not the only governing factors to characterize satellite precipitation uncertainty. Other factors, such as precipitation type, geographical proximity (location of the region from large water bodies etc.) play significant role on estimation of satellite precipitation uncertainty. A great deal of work remains to be done and we recommend further exploration to adequately address the issue of practical approaches to satellite precipitation uncertainty estimation in ungauged regions.

Acknowledgments

The authors thank the editor and all the anonymous reviewers who provided meaningful critique to significantly improve the quality of the presentation. The first author acknowledges the gracious support provided by NASA Earth System Science Fellowship (NNX12AN33H). Additional support from the NASA SERVIR program (NNX12AM85AG) is also acknowledged. The authors are also grateful to the generous support received from the Institute of Water Modeling (IWM) in Bangladesh and International Center for Integrated Mountain Development (ICIMOD) in Nepal, for access to quality controlled precipitation data as part of a long-standing MOU with University of Washington.

Appendix A. Performance measures

P_{EV}	predicted error variance
O_{EV}	observed error variance
n	number of sample size

Covariance, cov

$$\mathrm{cov}(P_{EV}, O_{EV}) = \sum_{i=1}^{n} \frac{\left(P_{EV}^{i} - \overline{P}_{EV}\right)\left(O_{EV}^{i} - \overline{O}_{EV}\right)}{n}. \tag{A1}$$

Correlation coefficient, r

$$r(P_{EV}, O_{EV}) = \frac{\mathrm{cov}(P_{EV} - O_{EV})}{\sigma_P \sigma_O}. \tag{A2}$$

Standard Error of Estimates, SEE

$$\mathrm{SEE} = \sqrt{\frac{\sum_{i=1}^{n}\left(P_{EV}^{i} - O_{EV}^{i}\right)^2}{n}}. \tag{A3}$$

Nash–Sutcliffe model efficiency coefficient, *E*

$$E = 1 - \frac{\sum_{i=1}^{n}\left(P_{EV}^{i} - O_{EV}^{i}\right)^2}{\sum_{i=1}^{n}\left(O_{EV}^{i} - \overline{O}_{EV}\right)^2}. \tag{A4}$$

Index of agreement, *d*

$$d = 1 - \frac{\sum_{i=1}^{n}\left(P_{EV}^{i} - O_{EV}^{i}\right)^2}{\sum_{i=1}^{n}\left(\left|P_{EV}^{i} - \overline{O}_{EV}\right| + \left|O_{EV}^{i} - \overline{O}_{EV}\right|\right)^2}. \tag{A5}$$

References

Adler, R.F., et al., 2003. The Version 2 Global Precipitation Climatology Project (GPCP) Monthly Precipitation Analysis (1979–Present). J. Hydrometeorol. 4, 1147–1167.

Artan, G., Gadain, H., Smith, J., Asante, K., Bandaragoda, C.J., Verdin, J., 2007. Adequacy of satellite derived precipitation data for streamflow modeling. Nat. Hazards 43, 167–185. http://dx.doi.org/10.1007/s11069-007-9121-6.

Bellerby, T., Sun, J., 2005. Probabilistic and ensemble representations of the uncertainty in an IR/microwave satellite precipitation product. J. Hydrometeorol. 6, 1032–1044.

Bowman, K.P., 2005. Comparison of TRMM precipitation retrievals with rain gauge data from ocean buoys. J. Climate 18, 178–190. http://dx.doi.org/10.1175/JCLI3259.1.

Chen, M., Shi, W., Xie, P., Silva, V.B.S., Kousky, V.E., Wayne, Higgins R., Janowiak, J.E., 2008. Assessing objective techniques for gauge-based analyses of global daily precipitation. J. Geophys. Res. 113, D04110. http://dx.doi.org/10.1029/2007JD009132.

Ciach, G.J., Krajewski, W.F., 1999. Radar-rain gauge comparisons under observational uncertainties. J. Appl. Meteorol. 38 (10), 1519–1525.

Fulton, R.A., Breidenbach, J.P., Seo, D.-J., Miller, D.A., O'Bannon, T., 1998. The WSR-88D precipitation algorithm. Weather Forecast. 13, 377–395.

Gebregiorgis, A.S., Hossain, F., 2013a. Estimation of Satellite precipitation error variance using readily available geophysical features. IEEE Trans. Geosci. Remote Sens. http://dx.doi.org/10.1109/TGRS.2013.2238636.

Gebregiorgis, A.S., Hossain, F., 2013b. Understanding the dependency of satellite precipitation uncertainty on topography and climate for hydrologic model simulation. IEEE Trans. Geosci. Remote Sens. 51 (1), 704–718.

Gebregiorgis, A.S., Tian, Y., Peters-Lidard, C., Hossain, F., 2012. Tracing hydrologic model simulation error as a function of satellite precipitation estimation bias components and land use and land cover conditions. Water Resour. Res. 48 (11). http://dx.doi.org/10.1029/2011WR011643 (p. W11 509).

Gebremichael, M., Krajewski, W.F., Morrissey, M., Langerud, D., Huffman, G.J., Adler, R., 2003. Error uncertainty analysis of GPCP monthly rainfall products: a data-based simulation study. J. Appl. Meteorol. 42, 1837–1848.

Gebremichael, M., Liao, G.Y., Yan, J., 2011. Nonparametric error model for a high resolution satellite rainfall product. Water Resour. Res. 47, W07504. http://dx.doi.org/10.1029/2010WR009667.

Haylock, M.R., Hofstra, N., Klein Tank, A.M.G., Klok, E.J., Jones, P.D., New, M., 2008. A European daily high-resolution gridded dataset of surface temperature and precipitation. J. Geophys. Res. Atmos. 113, D20119. http://dx.doi.org/10.1029/2008JD10201.

Hong, Y., Hsu, K., Gao, X., Sorooshian, S., 2004. Precipitation estimation from remotely sensed imagery using artificial neural network-cloud classification system. J. Appl. Meteorol. 43, 1834–1853.

Hong, Y., Hsu, K.-L., Moradkhani, H., Sorooshian, S., 2006. Uncertainty quantification of satellite precipitation estimation and Monte Carlo assessment of the error propagation into hydrologic response. Water Resour. Res. 42, W08421. http://dx.doi.org/10.1029/2005WR004398.

Hossain, F., Anagnostou, E.N., 2004. Assessment of current passive microwave- and infrared-based satellite precipitation remote sensing for flood prediction. J. Geophys. Res. 109 (D7) (p. D07 102).

Hossain, F., Shum, C.K., Turk, F.J., Biancamaria, S., Lee, H., Limaye, A., Mazumder, L.C., Hossain, M., Shah-Newaz, S., Ahmed, T., Yigzaw, W., Siddique-E-Akbor, A.H.M., 2014. A Guide for Crossing the Valley of Death: Lessons Learned From Making a Satellite Based Flood Forecasting System Operational and Independently Owned by a Stakeholder Agency. Bulletin of American Meteorological Society (BAMS) http://dx.doi.org/10.1175/BAMS-D-13-00176.1.

Hsu, K., Hong, Y., Sorooshian, S., 2007. Precipitation estimation using a cloud patch classification map. In: Levizzani, V., Bauer, P., Turk, F.J. (Eds.), Measurement of Precipitation From Space: EURAINSAT and Future. Springer Publishing Company, Dordrecht, pp. 329–343.

Huffman, G.J., 1997. Estimates of root mean square random error for finite samples of estimated precipitation. J. Appl. Meteorol. 36 (9), 1191–1201.

Huffman, G.J., Adler, R., Morrissey, M., Bolvin, D., Curtis, S., Joyce, R., McGavock, B., Susskind, J., 2001. Global precipitation at one-degree daily resolution from multisatellite observations. J. Hydrometeorol. 2, 36–50.

Huffman, G.J., Adler, R.F., Bolvin, D.T., Gu, G.J., Nelkin, E.J., Bowman, K.P., Hong, Y., Stocker, E.F., Wolff, D.B., 2007. The TRMM Multisatellite Precipitation Analysis (TMPA): quasi-global, multiyear, combined-sensor precipitation estimates at fine scales. J. Hydrometeorol. 8 (1), 38–55.

Huffman, G.J., Adler, R.F., Bolvin, D.T., Nelkin, E.J., 2010. The TRMM Multisatellite Precipitation Analysis (TMPA). In: Gebremichael, M., Hossain, F. (Eds.), Satellite Precipitation Applications for Surface Hydrology. Springer Publications, New York, pp. 3–22.

Iguchi, T., Kozu, T., Meneghini, R., Awaka, J., Okamoto, K., 2000. Rain-profiling algorithm for the TRMM precipitation radar. J. Appl. Meteorol. 39 (12), 2038–2052.

Joyce, R., Janowiak, J.E., Arkin, P.A., Xie, P., 2004. CMORPH: a method that produces global precipitation estimates from passive microwave and infrared data at high spatial and temporal resolution. J. Hydrometeorol. 5, 487–503.

Kidd, C., Kniveton, D.R., Todd, M.C., Bellerby, T.J., 2003. Satellite precipitation estimation using combined passive microwave and infrared algorithms. J. Hydrometeorol. 4, 1088–1104.

Kuligowski, R.J., 2002. A self-calibrating real-time GOES precipitation algorithm for short-term precipitation estimates. J. Hydrometeorol. 3, 112–130.

Lazri, M., Ameur, S., Brucker, J.M., Quallouche, F., 2014. Convective rainfall estimation from MSG/SEVIRI data based on different development phase duration of convective systems (growth phase and decay phase). Atmos. Res. 147–148 (2014), 38–50. http://dx.doi.org/10.1016/j.atmosres.2014.04.019.

Legates, D.R., McCabe Jr., G.J., 1999. Evaluating the use of "goodness-of-fit" measures in hydrologic and hydroclimatic model validation. Water Resour. Res. 35 (1), 233–241.

Lin, Y., Mitchell, K., 2005. The NCEP stage II/IV hourly precipitation analyses: Development and applicationsPreprints, 19th Conf. on Hydrology 1.2. Amer. Meteor. Soc, San Diego, CA (Available online at ams.confex.com/ams/Annual2005/ techprogram/paper_83847.htm.).

Maddox, R., Zhang, J., Gourley, J., Howard, K., 2002. Weather radar coverage over the contiguous United States. Weather Forecast. 17, 927–934.

Maggioni, V., Sapiano, M.R.P., Adler, R.F., Tian, Y., Huffman, G.J., 2014. An error model for uncertainty quantification in high-time-resolution precipitation products. J. Hydrometeorol. 15, 1274–1292. http://dx.doi.org/10.1175/JHM-D-13-0112.1.

Maurer, E.P., Wood, A.W., Adam, J.C., Lettenmaier, D.P., 2002. A long-term hydrologically based dataset of land surface fluxes and states for the conterminous United States. J. Climate 15, 3237–3251.

Miller, S.W., Arkin, P.A., Joyce, R., 2001. A combined microwave/infrared rain rate algorithm. Int. J. Remote Sens. 22 (17), 3285–3307.

Nash, J.E., Sutcliffe, J.V., 1970. River flow forecasting through conceptual models, part I — a discussion of principles. J. Hydrol. 10, 282–290.

Nijssen, B., Lettenmaier, D.P., 2004. Effect of precipitation sampling error on simulated hydrological fluxes and states: anticipating the global precipitation measurement satellites. J. Geophys. Res. 109 (D2), D02103. http://dx.doi.org/10.1029/2003JD003497.

North, G.R., Shen, S.S.P., Upson, R., 1993. Sampling errors in precipitation estimates by multiple satellites. J. Appl. Meteorol. 32, 399–410.

Pan, M., Li, H., Wood, E., 2010. Assessing the skill of satellite based precipitation estimates in hydrologic applications. Water Resour. Res. 46, W09535. http://dx.doi.org/10.1029/2009WR008290.

Romilly, T.G., Gebremichael, M., 2011. Evaluation of satellite rainfall estimates over Ethiopian river basins. Hydrol. Earth Syst. Sci. 15, 1505–1514. http://dx.doi.org/10.5194/hess-15-1505-2011.

Sapiano, M.R.P., Arkin, P.P., 2009. An intercomparison and validation of high-resolution satellite precipitation estimates with 3-hourly gauge data. J. Hydrometeor. 10, 149–166. http://dx.doi.org/10.1175/2008JHM1052.1.

Shiklomanov, A.I., Lammers, R.B., Vorosmarty, C.J., 2002. Widespread decline in hydrological monitoring threatens pan-arctic research. EOS Trans. 83, 16–17.

Shrestha, M.S., Artan, G.A., Bajracharya, S.R., Sharma, R.R., 2008. Using satellite-based precipitation estimates for streamflow modeling: Baghmati Basin. J. Flood Risk Manage 1, 89–99. http://dx.doi.org/10.1111/j.1753-318X.2008.00011.x.

Sorooshian, S., Hsu, K., Gao, X., Gupta, H.V., Imam, B., Braithwaite, D., 2000. Evolution of the PERSIANN system satellite-based estimates of tropical precipitation. Bull. Am. Meteorol. Soc. 81 (9), 2035–2046.

Sorooshian, S., Aghakouchak, A., Arkin, P., Eylander, J., Foufoula-Georgiou, E., Harmon, R., Hendrickx, J.M.H., Imam, B., Kuligowski, R., Skahill, B., Skofronick-Jackson, G., 2011. Advanced concepts on remote sensing of precipitation at multiple scales. Bull. Am. Meteorol. Soc. 92 (10), 1353–1357.

Stokstad, E., 1999. Scarcity of rain, stream gages threatens forecasts. Science 285, 1199.

Su, F.G., Hong, Y., Lettenmaier, D.P., 2008. Evaluation of TRMM Multisatellite Precipitation Analysis (TMPA) and its utility in hydrologic prediction in La Plata basin. J. Hydrometeor. 9, 622–640.

Su, F.G., Gao, H., Huffman, G.J., Lettenmaier, D.P., 2011. Potential utility of the real-time TMPA-RT precipitation estimates in streamflow prediction. J. Hydrometeor. 12, 444–455.

Tian, Y., Peters-Lidard, C.D., 2010. A global map of uncertainties in satellite-based precipitation measurements. Geophys. Res. Lett. 37 (24), L24407. http://dx.doi.org/10.1029/2010GL046008.

Tian, Y., Peters-Lidard, C.D., Eylander, J.B., Joyce, R.J., Huffman, G.J., Adler, R.F., Hsu, K., Turk, F.J., Garcia, M., Zeng, J., 2009. Component analysis of errors in satellite-based precipitation estimates. J. Geophys. Res. 114, D24101. http://dx.doi.org/10.1029/2009JD011949.

Tong, K., Su, F., Yang, D., Zhang, L., Hao, Z., 2013. Tibetan Plateau precipitation as depicted by gauge observations, reanalyses and satellite retrievals. Int. J. Climatol. http://dx.doi.org/10.1002/joc.3682.

Wilks, D.S., 2011. Statistical Methods in the Atmospheric Sciences, 3rd ed. 215–300. Academic Press, pp. 3–19. http://dx.doi.org/10.1016/B978-0-12-385022-5.00001-4.

Willmot, C.J., 1981. On the validation of models. Phys. Geogr. 2, 184–194.

Wu, H., Adler, R.F., Hong, Y., Tian, Y., Policelli, F., 2012. Evaluation of global flood detection using satellite-based precipitation and a hydrologic model. J. Hydrometeor 13, 1268–1284.

Xie, P., Yatagai, A., Chen, M., Hayasaka, T., Fukushima, Y., Liu, C., Yang, S., 2007. A gauge-based analysis of daily precipitation over East Asia. J. Hydrometeor 8, 607–627.

Yan, J., Gebremichael, M., 2009. Estimating actual rainfall from satellite rainfall products. Atmos. Res. 92, 481–488. http://dx.doi.org/10.1016/j.atmosres.2009.02.004.

Yatagai, A., Kamiguchi, K., Arakawa, O., Hamada, A., Yasutomi, N., Kitoh, A., 2012. APHRODITE: constructing a long-term daily gridded precipitation dataset for Asia based on a dense network of rain gauges. Bull. Am. Meteorol. Soc. http://dx.doi.org/10.1175/BAMS-D-11-00122.1.

Zhang, X., Anagnostou, E.N., Frediani, M., Solomos, S., Kallos, G., 2013. Using NWP simulations in satellite rainfall estimation of heavy precipitation events over mountainous areas. J. Hydrometeor 14, 1844–1858.